

2

MARTIN MARIETTA ENERGY SYSTEMS LIBRARIES



3 4456 0365439 2

ORNL-3431  
 UC-28 – Particle Accelerators and  
 High-Voltage Machines  
 TID-4500 (20th ed.)

A STRONG-FOCUSING CYCLOTRON WITH  
 SEPARATED ORBITS  
 F. M. Russell

**CENTRAL RESEARCH LIBRARY  
 DOCUMENT COLLECTION  
 LIBRARY LOAN COPY**  
**DO NOT TRANSFER TO ANOTHER PERSON**  
 If you wish someone else to see this  
 document, send in name with document  
 and the library will arrange a loan.



**OAK RIDGE NATIONAL LABORATORY**  
 operated by  
**UNION CARBIDE CORPORATION**  
 for the  
**U.S. ATOMIC ENERGY COMMISSION**

Printed in USA. Price: \$2.00 Available from the  
Office of Technical Services  
U. S. Department of Commerce  
Washington 25, D. C.

#### LEGAL NOTICE

This report was prepared as an account of Government sponsored work. Neither the United States, nor the Commission, nor any person acting on behalf of the Commission:

- A. Makes any warranty or representation, expressed or implied, with respect to the accuracy, completeness, or usefulness of the information contained in this report, or that the use of any information, apparatus, method, or process disclosed in this report may not infringe privately owned rights; or
- B. Assumes any liabilities with respect to the use of, or for damages resulting from the use of any information, apparatus, method, or process disclosed in this report.

As used in the above, "person acting on behalf of the Commission" includes any employee or contractor of the Commission, or employee of such contractor, to the extent that such employee or contractor of the Commission, or employee of such contractor prepares, disseminates, or provides access to, any information pursuant to his employment or contract with the Commission, or his employment with such contractor.

ORNL-3431

Contract No. W-7405-eng-26

ELECTRONUCLEAR DIVISION

A STRONG-FOCUSING CYCLOTRON WITH SEPARATED ORBITS

F. M. Russell

January 1963

DATE ISSUED

JUN 28 1963

OAK RIDGE NATIONAL LABORATORY

Oak Ridge, Tennessee

Operated by

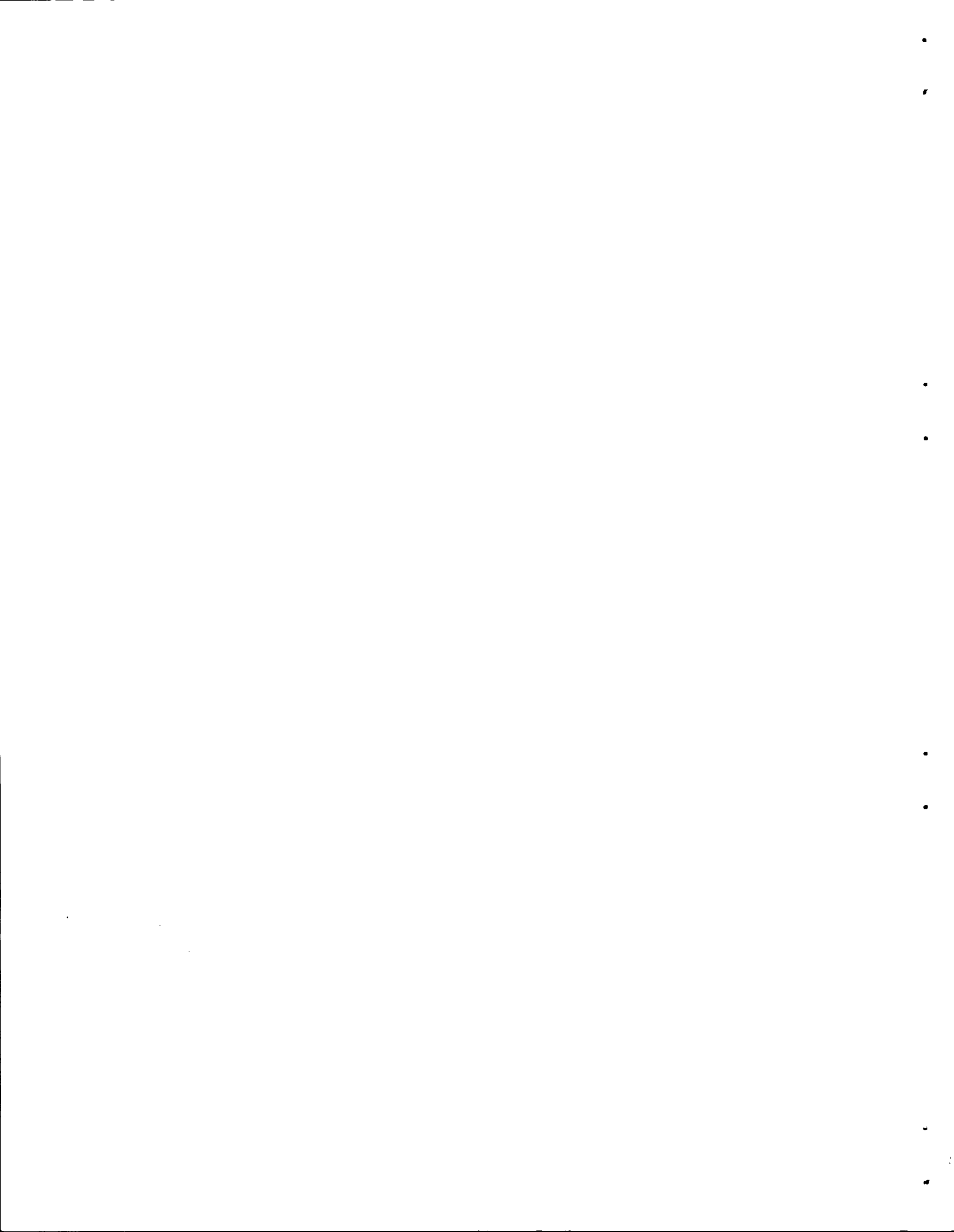
UNION CARBIDE CORPORATION

for the

U. S. ATOMIC ENERGY COMMISSION



3 4456 0365439 2



A Strong-Focusing Cyclotron with Separated Orbits

F. M. Russell\*

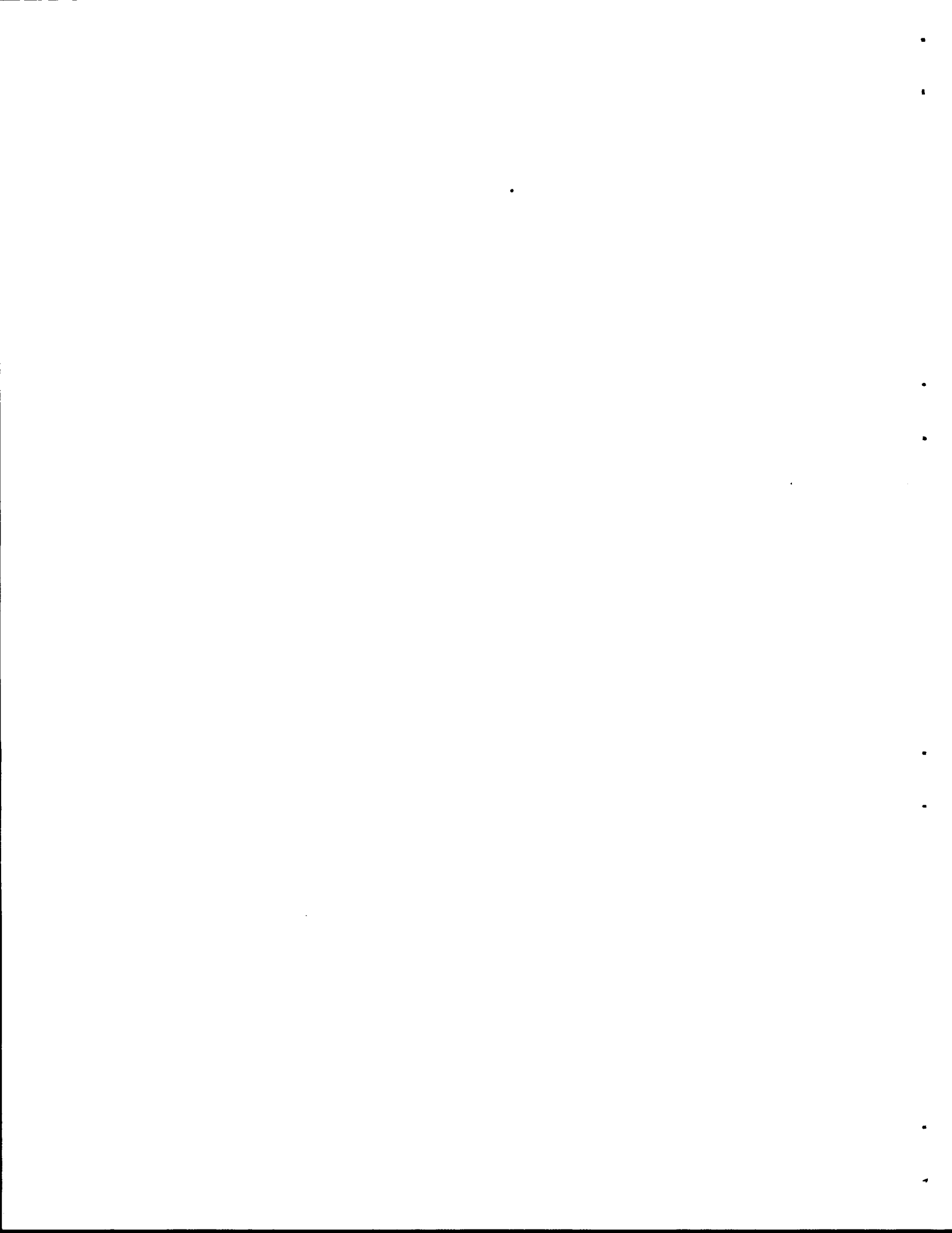
Oak Ridge National Laboratory

Abstract

The concept and basic theory of a new fixed-frequency, fixed-field, high-energy accelerator embodying the principle of strong-focusing and capable of accelerating protons to energies in the GeV region is described. The magnetic field is designed with the turns of the 'equilibrium orbit' separated axially as well as radially, as in a spiral-helix, so as to avoid the resonances associated with alternating-gradient systems. The focusing properties can be changed discontinuously at chosen points along the orbit to avoid the error resonances. Longitudinal stability is present, as the system is phase stable. Ions spiral repeatedly through several accelerating cavities operated in the TE mode and spaced regularly around the machine. Each cavity extends both radially and axially to intercept all turns only once. Injection and extraction are straight-forward and the final energy can be varied by extracting at chosen points along the orbit path. A preliminary design for a 1-GeV machine is described, and a comparison is made between the proposed machine and some contemporary types of accelerators. The cost estimate compares favorably with that of other machines with which it is compared.

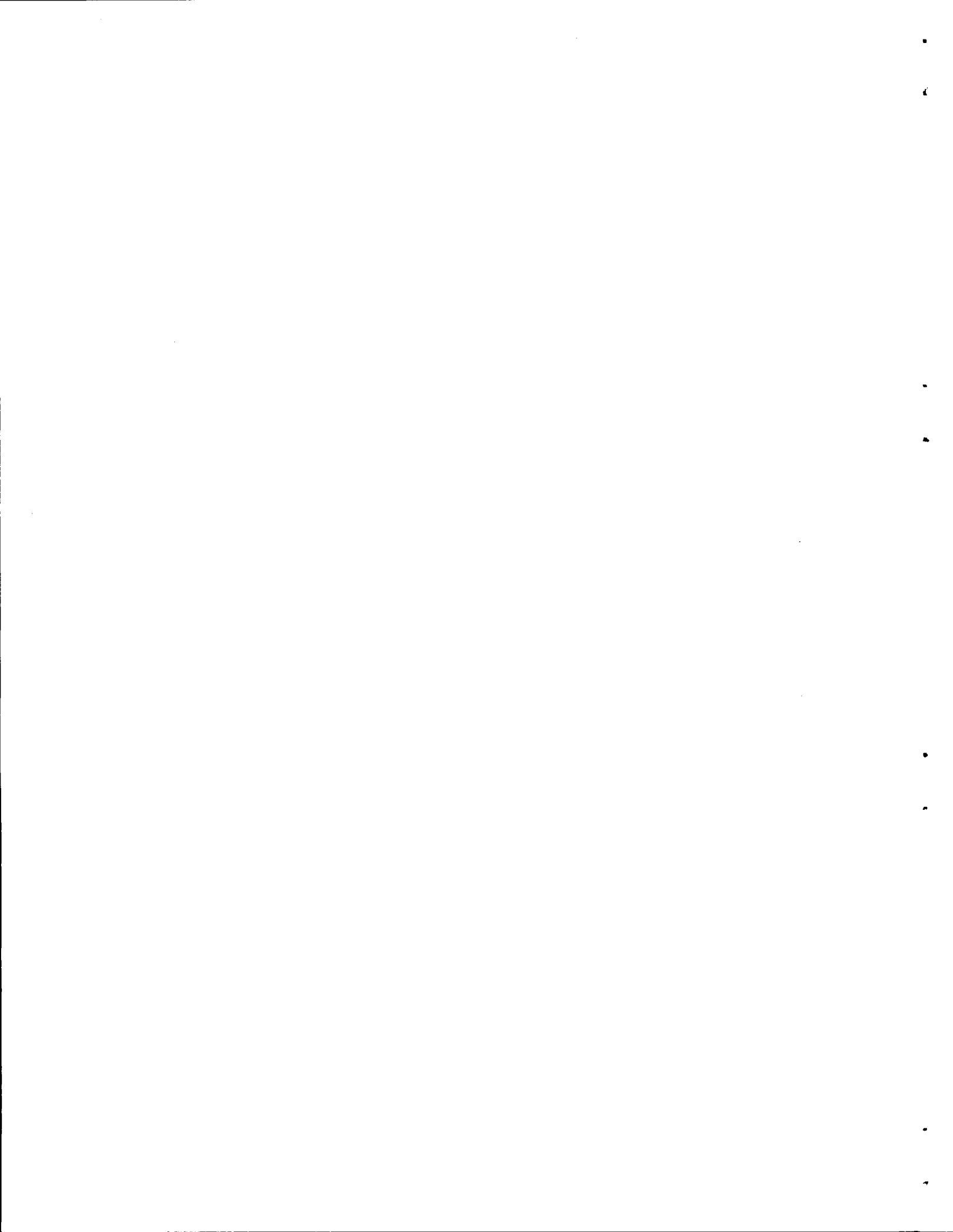
---

\*Visiting scientist, Electronuclear Division, from Rutherford High Energy Laboratory, Harwell.



Contents

1.	Introduction - - - - -	1
2.	The Equilibrium Orbit (Smooth Approximation) - - - - -	2
	2.1. Inclusion of Radio-Frequency Gaps - - - - -	5
	2.2. Inclusion of Straight Sections - - - - -	7
3.	Stability of Motion - Transverse - - - - -	8
	3.1. Basic Instabilities - - - - -	9
	3.2. Field Errors - - - - -	12
4.	Longitudinal Stability - - - - -	14
5.	Effects of the Radio-Frequency Gaps - - - - -	17
	5.1. Gap Defocusing - - - - -	17
	5.2. Orbit Tilt - - - - -	18
	5.3. Transit Time - - - - -	18
6.	Tolerances - - - - -	19
	6.1. Single Cell Error - - - - -	19
	6.2. Double Cell Error - - - - -	20
	6.3. Smooth Errors - - - - -	21
	6.4. Mean Field and Frequency Errors - - - - -	22
7.	The RF System - - - - -	23
8.	The Magnet - - - - -	28
9.	Logical Developments - - - - -	30
10.	Tune-Up Procedure - - - - -	32
11.	Applications - - - - -	33
12.	Design of a 1-GeV Machine - - - - -	35
	12.1. The 120 - 1,000 MeV SOC, Basic Design - - - - -	35
	12.2. The 15 - 120 MeV SOC, Basic Design - - - - -	39
	12.3. Cost Estimate for SOC System, Initial Design - - - - -	42
13.	Development of a Proposed SOC - - - - -	44
	13.1. A Developed Design for a 120-MeV to 1-GeV SOC - - - - -	64
	13.2. Cost Estimate for 1-GeV SOC System, Developed Design - - - - -	68
	13.3. Three Types of High-Intensity Accelerators (Meson Factories) Briefly Compared - - - - -	71



## 1. Introduction

The subject of this report is an accelerator which appears well suited to applications in the intermediate range of particle energies, ranging from about 15 MeV up to several GeV. The basic idea was conceived in 1958 but, beyond a brief notation of the apparent feasibility of the idea, it was not then pursued. The growth of interest in high intensity, intermediate energy accelerators in recent years has, however, stimulated a more careful study. Late in 1962 a short article was prepared describing the basic features<sup>(1)</sup>. The preliminary study which followed is here reported.

A simple approximate theory of the machine is first derived. This is followed by a brief study of stability of particle motion in both transverse and longitudinal directions. Various types of machine errors are examined in connection with stability of motion. Specific components of the machine then are examined.

By way of illustration, in Sec. 12, a tentative design is developed for an accelerator system capable of producing a 1-mA beam of protons at an energy of 1 GeV. The components of this system are described in some detail and a cost estimate is prepared.

Further examination and developed of the separated-orbit concept, Sec. 13, indicate a number of improvements and simplifications which, when applied to the design of the accelerator, provide for a more compact system and also reduce the cost estimate.

For simplicity the machine herein described will be referred to as a Separated Orbit Cyclotron, or SOC.

## 2. The Equilibrium Orbit (Smooth Approximation)

Let us assume that an equilibrium orbit exists and that an ion on this orbit moves along a curve resembling a helix of increasing radius. Such a path is indicated schematically in Fig. 1. Let the equilibrium orbit be intersected by a number of planes whose common line of intersection lies along the z-axis and which are equally spaced in azimuth about the z-axis. Assume that at each point of intersection of these planes with the equilibrium orbit there is applied an rf accelerating electric field directed along the equilibrium orbit.

Let all the rf electric fields at a given azimuth be in phase and let there be  $2N$  such acceleration gaps per turn ( $N$  planes). If the amplitudes of the rf gap voltages are maintained constant, then the rotational frequency of an ion on the equilibrium orbit can be made constant by suitable programming of the equilibrium orbit path in space.

Neglecting temporarily the small increase in path length per turn introduced by the shallow helix, then the path of the equilibrium orbit can be computed easily. Let  $\Delta E$  be the energy gain per gap crossing, then after the  $a$ 'th gap the total energy is

$$E = E_0 + T,$$

where  $E_0$  is the rest energy and

$$T = a \Delta E + E \text{ (initial)}.$$

If the velocity of the ion is then  $V_a$ , and it is moving in a magnetic field of mean strength  $B_a$  with a radius of curvature  $r_a$ , then

$$V_a = \frac{e}{m_a} r_a B_a .$$

Let the time between successive accelerations be  $\tau_a$ , then

$$\theta_a = \frac{V_a}{r_a} \tau_a = \frac{e}{m_a} B_a \tau_a . \quad (1)$$

For operation at a constant rotational frequency put  $\theta_a$  equal to a constant value  $\theta_c$ , where

$$\theta_c = 2\pi f_0 \tau_a ,$$

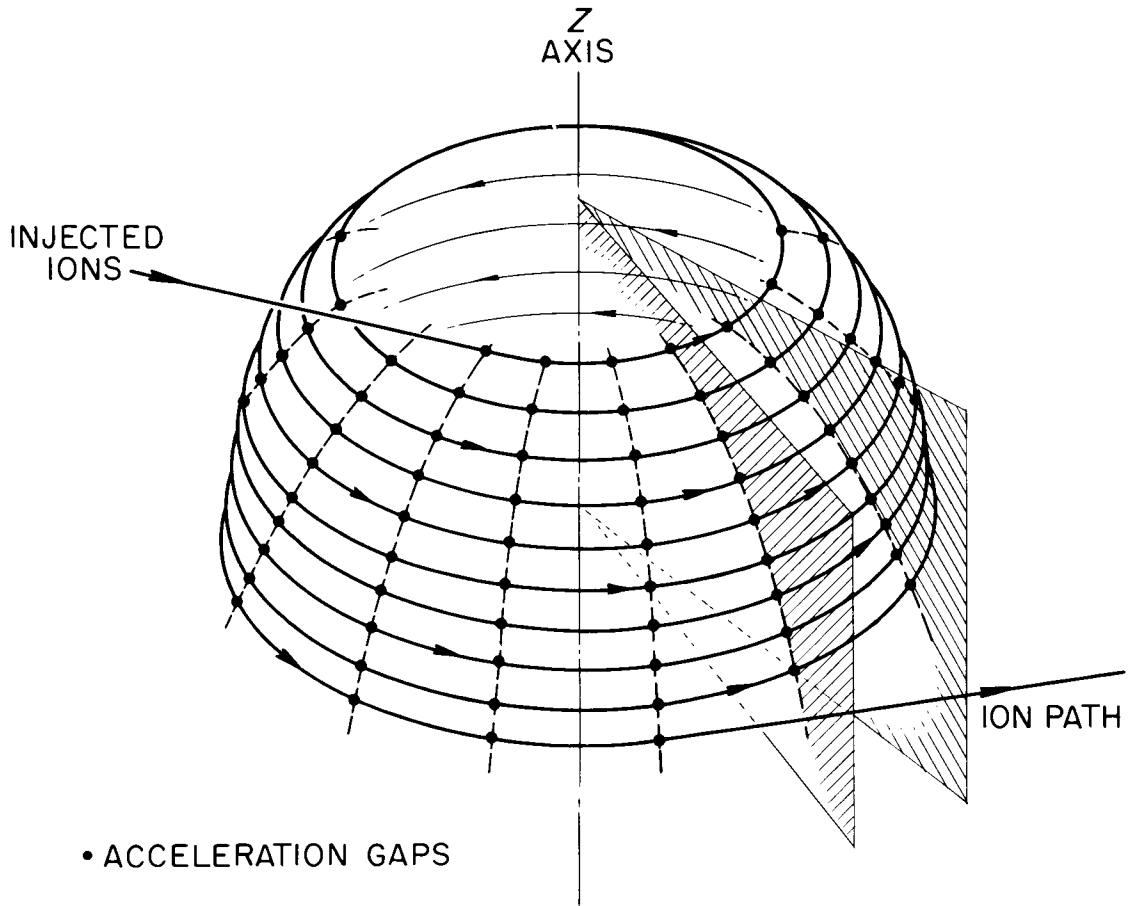
UNCLASSIFIED  
ORNL-LR-DWG 74595R

Fig. 1. Diagram of beam path with both radial and axial separation. Accelerating gaps are indicated by dots along the beam path. The rf voltages at the gaps joined by dashed line are in phase.

and the 'cyclotron frequency'  $f_0$  is

$$f_0 = \frac{B_a e}{2\pi m_a} .$$

The radius of curvature in the  $a$ 'th sector is given by the usual expression

$$r_a = (1 - 1/\gamma_a^2)^{1/2} R, \quad (2)$$

where

$$\gamma = E/E_0,$$

and  $R$  is the 'cyclotron radius' given by

$$R = c/2\pi f_0.$$

To maintain isochronism the mean magnetic field strength must vary as

$$B_a = \gamma_a B_0 ,$$

where

$$B_0 R = c m_0/e.$$

Provided that movement of the instantaneous orbit center is small, that is,  $T \gg \Delta E$ , then the radius of the equilibrium orbit in the smooth approximation is given by Eq.(2).

The displacement in the  $z$  direction during each turn causes a slight increase in the orbit path unless the radius is changed. For most practical cases where  $r_a \gg \Delta Z$ , where  $\Delta Z$  is the  $z$  displacement per turn, the increase in orbit length is small and corresponds to a fractional increase of

$$\frac{1}{2} \left( \frac{\Delta Z}{2\pi r_a} \right)^2 .$$

Ideally, a linear motion is required in the  $z$ -direction. If  $L$  is the length along the equilibrium orbit, then

$$L = \int r_a d\theta ,$$

and, as

$$\frac{T}{E_0} = \frac{\Delta E}{E_0} \frac{\theta}{\theta_c}, \quad (E_{\text{initial}} = 0),$$

so that

$$d\theta = \theta_c \frac{E_0}{\Delta E} dy$$

then

$$L = \frac{R \theta_c E_0}{\Delta E} \int \frac{\sqrt{\gamma^2 - 1}}{\gamma} dy.$$

Integrating

$$z(\gamma) = D(z) \frac{R \theta_c E_0}{\Delta E} \left\{ \sqrt{\gamma^2 - 1} - \cos^{-1} \left| 1/\gamma \right| \right\},$$

where

$$D(z) = \frac{dz}{dL}$$

is the chosen slope.

## 2.1 Inclusion of Radio-Frequency Gaps

Let the gap width along the equilibrium orbit be constant for all gaps; this is reasonable since  $\Delta E$  is assumed constant. Idealizing to the case of no magnetic fringing field then from the construction in Fig. 2 it is apparent that  $\theta_c' = \theta_c$ . Let us assume that the time interval  $\tau_a$  is unchanged by the inclusion of the gaps, each width  $2g$ . Consequently, the linear paths between gap centers is unchanged so that

$$\theta_c r_a' + 2g = \theta_c r_a, \quad (4)$$

and so

$$r_a' = (r_a - 2g/\theta_c). \quad (5)$$

The distance between the new center of curvature and the machine axis is  $(0, 0')$ , which for  $T \gg \Delta E$  is given by

$$(0, 0') = g/\sin(\theta_c/2).$$

The radius to the orbit at the gap center is

$$r_a' + g/\tan(\theta_c/2),$$

UNCLASSIFIED  
ORNL-LR-DWG 76868

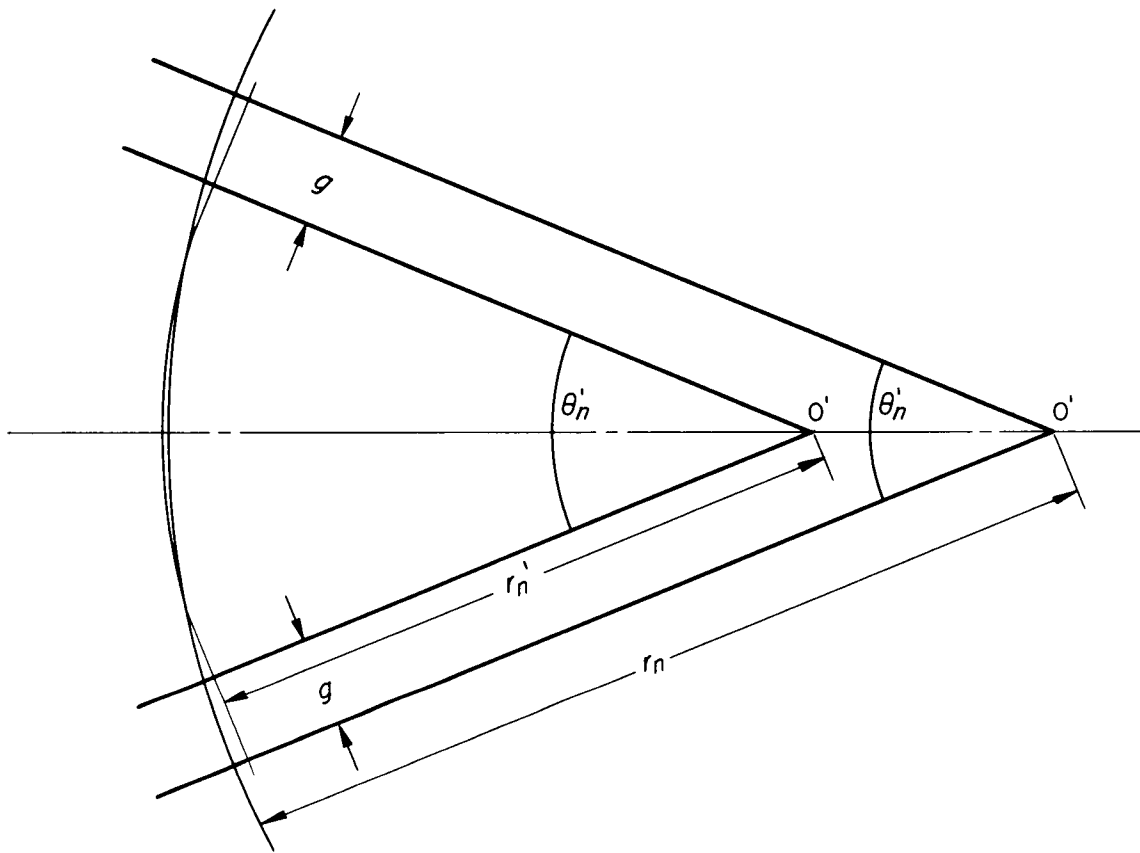


Fig. 2. Drawing showing the radii of curvature of the orbits, when field-free gaps are absent and when they are present.

and so the introduction of the gaps causes the orbits to move inwards at the gap centers by an amount  $\delta_r$  where

$$\delta_r = g \left( \frac{1}{(\theta_c/2)} - \frac{1}{\tan(\theta_c/2)} \right). \quad (6)$$

Since  $g$  and  $\theta_c$  are assumed constant, then  $\delta_r$  is constant, too.

From the condition of unchanged momentum

$$B_a' / B_a = r_a / r_a'$$

and so

$$B_a' = \frac{B_o \gamma}{(1 - q)}, \quad (7)$$

where

$$q = 2g/r_a \theta_c.$$

Equation (7) shows that at low energies the magnetic field strength must be increased to compensate for the increased fraction of the orbit taken up by the gaps, while at high energies the normal increase with  $\gamma$  is found.

It is apparent that the new orbit oscillates about an orbit for the no-gap condition with amplitude limits of

$$\left. \begin{array}{l} + g (1/\sin x - 1/x) \\ - g (1/x - 1/\tan x) \end{array} \right\},$$

where  $x = \theta_a/2$ .

## 2.2 Inclusion of Straight Sections

If straight sections are introduced into the orbits at fixed azimuthal positions, as required in sections 9 and 13, then to maintain the condition of constant rotational frequency it is necessary to change the strength of the magnetic field in each cell. To maintain synchronism with the rf the straight sections must be, or occupy, an integral number of half-periods.

Let the number of half-periods per straight section be  $\Gamma$ , then Eq. (7) is modified to

$$B_a' = \frac{B_o \gamma}{(1 - q)(1 - p)} \quad (8)$$

where

$$p = \frac{2\Gamma \beta \lambda_o}{\pi r_a}.$$

### 3. Stability of Motion - Transverse

In any accelerator it is necessary for some restoring force to act upon ions which deviate from the equilibrium orbit. Of the two basic types, 'weak' and 'strong' focusing, it is natural to favor the latter because of the smaller apertures required. However, the potentially enormous savings in aperture which should accompany strong focusing are not usually achieved. This is because of the many resonances that can occur between the ions and certain periodicities in the guiding field, causing growth of betatron oscillation amplitudes in time and subsequent loss of ions to the chamber walls.

If, however, the ions pass any given point in the machine only once during the entire process of acceleration, then many of the resonances associated with strong-focusing machines are eliminated. It is apparent that the helical path of the assumed equilibrium orbit in the proposed machine is of the single-pass type. Ideally, if there is no coupling between turns, then all the integral, subintegral, and error resonances can be eliminated; even the coupling resonances could be avoided. This result follows from the fact that the 'working point' on the stability diagram can move in a discontinuous manner, jumping over a resonance line if necessary, because the magnetic field gradients can be changed in a discontinuous way at chosen points along the orbit.

In the ideal case, therefore, only the basic instabilities common to all AG systems exist, and these present no difficulty in design. Random errors or misalignments will, however, be important in any practical machine. Of importance are the permissible tolerances on position and gradients which will just allow the beam to pass through a given aperture after a given path length.

### 3.1. Basic Instabilities

The theory of ion motion in alternating gradient fields is well understood.<sup>(3)</sup> In consequence, results of the theory will simply be quoted where appropriate.

Let  $n$  be the field index, defined as

$$n = - \frac{r}{B(r)} \frac{dB_z}{dr} ,$$

and let its value in the  $a$ 'th subcell on the equilibrium orbit be  $n_a$ . The length of the  $a$ 'th subcell is  $L_a$  where

$$L_a = r_a \theta_c - 2g. \quad (9)$$

Motion within a cell consisting of one gap and one magnet cell of constant  $n$  can be described by using matrix methods, given the coordinates and transverse velocity prior to entry to the cell.

The matrix for a cell with  $n > 0$  is

$$M_a = \begin{bmatrix} \cos \psi_a - 2gX_a \sin \psi_a & \frac{1}{X_a} \sin \psi_a + 2g \cos \psi_a \\ -X_a \sin \psi_a & \cos \psi_a \end{bmatrix} , \quad (10)$$

and for the next cell, for which  $n < 0$

$$M_{(a+1)} = \begin{bmatrix} \cosh \psi_{a+1} + 2g X_{a+1} \sinh \psi_{a+1} & \frac{1}{X_{a+1}} \sinh \psi_{a+1} + 2g \cosh \psi_{a+1} \\ X_{a+1} \sinh \psi_{a+1} & \cosh \psi_{a+1} \end{bmatrix} , \quad (11)$$

where

$$\psi_a = X_a L_a ,$$

and

$$X_a = \sqrt{\frac{n_a}{r_a}} .$$

The trace of the produce matrix  $M_a M_{a+1}$  is given by

$$\begin{aligned} T_r M &= 2 \cos \Psi_a \cosh \Psi_{a+1} + 4gX_{a+1} \cos \Psi_a \sinh \Psi_{a+1} \\ &\quad - 4gX_a \sin \Psi_a \cosh \Psi_{a+1} - 4g^2 X_a X_{a+1} \sin \Psi_a \\ &\quad \sinh \Psi_{a+1} + \sin \Psi_a \sinh \Psi_{a+1} \left( \frac{X_{a+1}}{X_a} - \frac{X_a}{X_{a+1}} \right). \end{aligned} \quad (12)$$

Defining a quantity  $\sigma$  by the relation

$$2 \cos \sigma = T_r M \quad (13)$$

then the basic condition for stability of transverse motion is that  $\sigma$  is real. It is noted in passing that from Eqs. (5) and (9)

$$L_a / r_a' = \theta_c = \pi / N, \quad (14)$$

where  $2N$  is the number of cells per turn. The familiar 'necktie' diagram indicating the region of stable motion in terms of  $n_a / N^2$  and  $n_{a+1} / N^2$  is shown in Fig. 3.

The preceding results are not strictly applicable because of the small but finite 'twist' in the orbit produced by the helical motion. The rate of twist is given by

$$d\mu / dL = D(z) / r_a', \quad (15)$$

where the slope  $D(z) = dz / dL$ , and  $\mu$  is the angle of twist in the length  $L$ . This topic is examined in Section 3.2.

Since  $\sigma$ , as given by Eq. (13), is the phase change per pair of cells and straight sections the frequency of the betatron oscillations can be found, from which the  $\nu$  values are

$$\nu_z = \frac{N\sigma_z}{2\pi}, \quad \text{and} \quad \nu_r = \frac{N\sigma_r}{2\pi},$$

where  $\sigma_r$  and  $\sigma_z$  are derived from Eq. (13) by interchanging  $n_a$  and  $n_{a+1}$ . It should be remembered that  $\nu_z$  refers to transverse motion in a direction perpendicular to the radial transverse motion.

UNCLASSIFIED  
ORNL-LR-DWG 76869

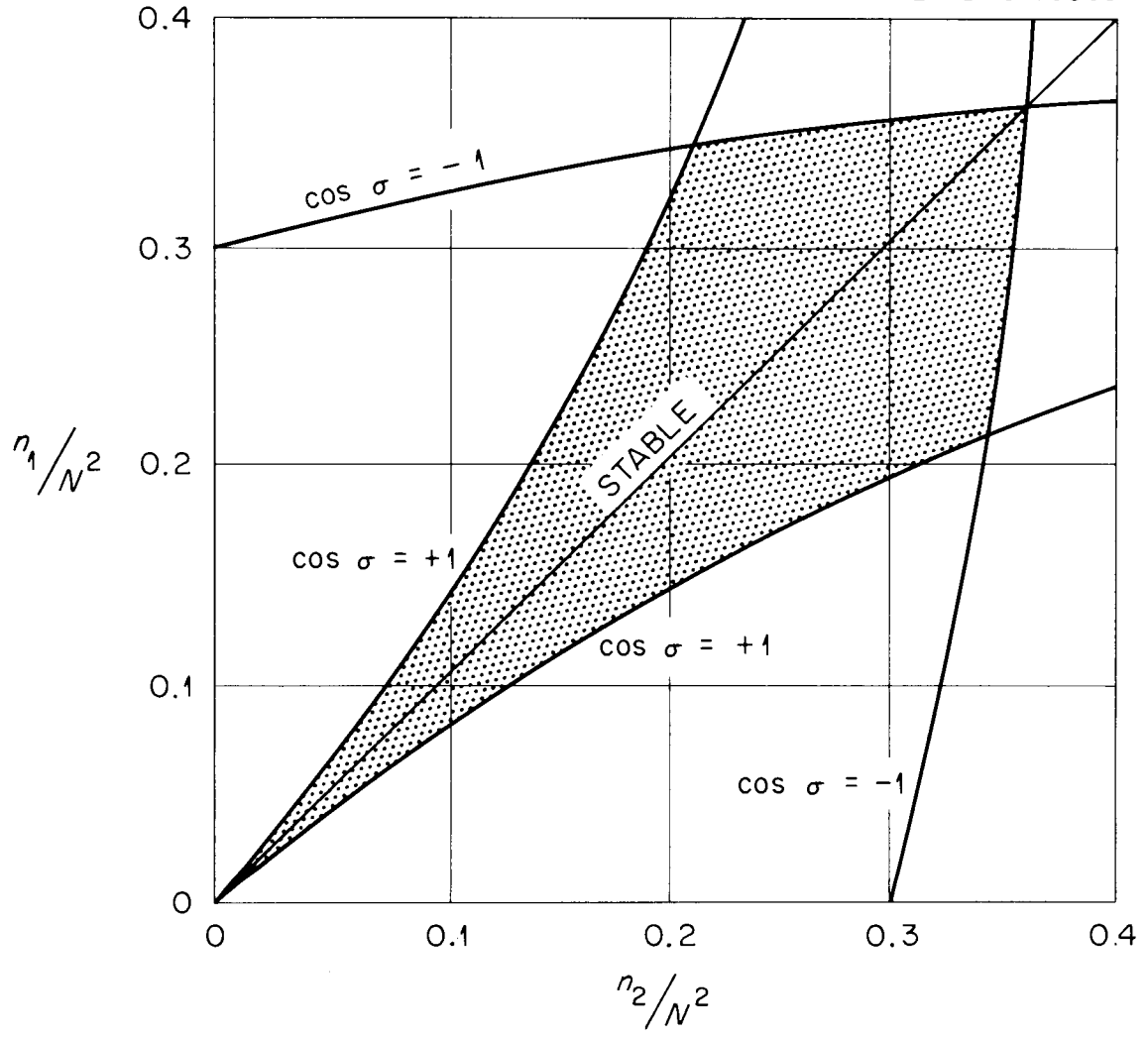


Fig. 3. 'Necktie' diagram showing the regions of stability.

If we cause  $n_a$  to vary with  $(r_a')^2$  so that  $X_a = X_{a+1} = X_o$  then Eq. (12) reduces to

$$\begin{aligned} T_r M = & 2 \cos \Psi_1 \cosh \Psi_2 + 4gX_o (\cos \Psi_1 \sinh \Psi_2 - \sin \Psi_1 \cosh \Psi_2) \\ & - 4g^2 X_o^2 \sin \Psi_1 \sinh \Psi_2 , \end{aligned} \quad (16)$$

where

$$\begin{aligned} \Psi_1 &= X_o L_a \\ \Psi_2 &= X_o L_{a+1} \end{aligned}$$

It is apparent that if  $n_a$  is varied in the above manner, then the  $v_z, v_r$  values change progressively during the acceleration.

### 3.2. Field Errors

If a perfect guide field could be constructed, then the upper limit on the field gradient would be set solely by the condition for stability. It is reasonable to ask, what are the physical advantages to be gained from using high field gradients?

To a good approximation the beam disturbances caused by displacements of ideal magnet cells from their correct locations are independent of the magnitudes of the field gradients for given displacements. However, for other field errors, such as nonuniform gradients, twists, and tilts about the equilibrium orbit, the amplitude of betatron oscillations is reduced as  $n$  is increased, at least to moderate  $n$  values. At some value of  $n$  the reduction in beam cross section caused by an increase in  $n$  will be offset by the errors introduced in creating the fields. The question of how rapidly the beam, say initially on the equilibrium orbit, spreads as a result of random field errors is very important; it fixes the accuracy with which elements should be made. Preliminary estimates indicate that tolerances on mechanical adjustment about the ideal or equilibrium orbit could be  $\pm 5 \times 10^{-3}$  in. The corresponding field error is about 1 in  $10^3$ , which is a moderately relaxed tolerance for a fixed field device.

The effect on tolerances of imposing the condition that adjustments can be made where necessary to 'tune' the system are simply not known. Some conclusions might be drawn in this respect from hand tuning of AVF cyclotrons.<sup>(4)</sup>

It has been pointed out\* that there is coupling between the two transverse motions caused by the twisting of the equilibrium orbit along the helix. The magnitude of this twist is given by

$$\mu = \int \frac{dZ}{dL} d\theta , \quad (17)$$

integrated over the equilibrium orbit. The effect of such coupling on beam stability is not obvious. If  $\nu_z = \nu_r$ , then energy can be transferred directly between the two transverse motions and corresponds to a coupling resonance. The result is that the two motions can become interchanged. In a strong-focusing system with  $\nu_z \sim \nu_r$  this would be a disadvantage only if the initial phase-space plots of the two motions were grossly dissimilar, or became so during acceleration to the final energy; some of the beam would probably be lost to the beam chamber.

If a linac is used for injection into an SOC, then the inherent cylindrical symmetry of a linac would be manifested in the injected beam and, by proper matching between the two parts, could be propagated into the SOC section.

It is a simple matter to make  $\nu_z$  and  $\nu_r$  different by suitable choice of  $n_a$  and  $n_{a+1}$ ; it might be desirable to avoid the coupling resonance in this way.

---

\*J. A. Martin, Electronuclear Division, Oak Ridge National Laboratory.

#### 4. Longitudinal Stability

The machine described here exhibits phase stability of motion with respect to the rf, provided that the rf voltage exceeds a given value. The major advantage of phase-stable motion is that nonsynchronous ions are successfully accelerated. The disadvantages are that ions on the average gain less than the maximum energy possible per gap crossing and that at all energies there is a spread in energy of the ions about that of the synchronous ion. As usual, the advantage far outweighs the disadvantages.

Only the outline of the theory of phase stability will be given here since the usual assumption of adiabatic changes in the machine parameters is not strictly true in the present case. The conditions prevailing more closely resemble those of a linear accelerator than those of a synchrotron as the rate of energy gain is high ( $\sim 20$  MeV/turn).

Let  $\alpha$  be the momentum compaction factor, defined as

$$\alpha = \frac{L}{p} \frac{dp}{dL} \quad , \quad (18)$$

where  $p$  and  $L$  are the momentum and length along orbit path respectively.

To a first approximation  $\alpha$  is given by

$$\alpha = \frac{n_a^{3/2}}{4N} \pi \left( 1 + \frac{2g}{L_a} \right) \left( \coth \Psi_a/2 - \cot \Psi_a/2 + 2g \Psi_a/L_a \right), \quad (19)$$

where

$$\Psi_a = \frac{\sqrt{n_a} \pi}{N} = \sqrt{n_a} (L_a/r_a') \quad .$$

From the relation

$$p^2 = T(T + 2 E_o)/c^2 \quad ,$$

and Eq. (18)

$$\frac{\delta L}{L} = \frac{1}{\alpha} \frac{E_o + T}{2 E_o + T} \frac{\delta T}{T} \quad . \quad (20)$$

The fractional change in the time  $\tau$  between successive accelerations is given by

$$\frac{\delta \tau}{\tau} = \frac{\delta L}{L} - \frac{1}{\gamma^2} \frac{\delta p}{p} ,$$

and so

$$\frac{\delta \tau}{\tau} = \left( \frac{1}{\alpha} - \frac{1}{\gamma^2} \right) \frac{E_0 + T}{2E_0 + T} \frac{\delta T}{T} .$$

The phase change per cycle of the rf,  $d\phi/dc$ , is thus given by

$$\frac{d\phi}{dc} = \Lambda 2\pi \frac{\Delta T}{T} , \quad (21)$$

where

$$\Lambda = \left( \frac{1}{\alpha} - \frac{1}{\gamma^2} \right) \frac{E_0 + T}{2E_0 + T} .$$

Since

$$\frac{dc}{dt} = \frac{\omega_s}{2\pi} = \frac{N \omega_0}{2\pi}$$

and the rate of change of the energy difference  $\Delta T$  is

$$\frac{d(\Delta T)}{dc} = E_1 (\cos \phi - \cos \phi_s),$$

where  $\phi_s$  is the phase-stable angle and

$$E_1 = eV_0 ,$$

then

$$\frac{d(\Delta T)}{d} = \frac{N \omega_0 E_1}{2\pi} (\cos \phi - \cos \phi_s). \quad (22)$$

From Eq. 21 and 22

$$\frac{d}{dt} \left( \frac{T}{N \omega_0 \Lambda} \frac{d\phi}{dt} \right) = \frac{N \omega_0 E_1}{2\pi} (\cos \phi - \cos \phi_s) \quad (23)$$

which is the usual equation describing phase-stable motion.

For the high energy region of an SOC it is reasonable to assume that both  $T$  and  $\Lambda$  change adiabatically. Solution of Eq. (23) for the angular frequency of small oscillation amplitudes then gives

$$\Omega = \left( \frac{E_1 \Lambda \cos \phi_s}{2\pi T} \right)^{1/2} N \omega_o . \quad (24)$$

At the low energy end, however,  $T/\Lambda$  is changing rapidly. The general trend can be found by computation. Principally, there are two effects, the frequency of oscillation  $\Omega$  and the amplitude of energy deviation  $\Delta E$  both decreasing with increasing  $E_s$ .

Some insight into the phase motion at low energies might be obtained by simplifying Eq. (23). The energy gain  $T$  oscillates about the synchronous value  $T_s$ , which is given by

$$T_s = 2 t \left( \frac{N \omega_o}{2\pi} \right) E_1 \cos \phi_s ,$$

if  $E_1$  and  $\phi_s$  are constant. Neglecting the oscillation of  $T$  about  $T_s$  then

$$\frac{d}{dt} \left( t \frac{d\phi}{dt} \right) = \frac{N \omega_o}{4 \cos \phi_s} (\cos \phi - \cos \phi_s) . \quad (25)$$

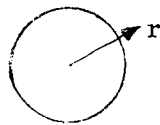
## 5. Effects of the Radio Frequency Gaps

Several factors affecting the ion motion arise at the necessary holes or gaps in the rf cavities across which the electric accelerating fields are generated.

### 5.1. Gap Defocusing

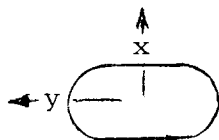
If the phase-stable angle is negative, as is required for stable longitudinal motion, then ions experience a defocusing force at each gap crossing. We will assume that the space-charge density of the ions crossing the gap is sufficiently small that Laplace's equation can be used to describe the instantaneous field pattern in the vicinity of a gap.

It is interesting to note that the defocusing force can be made non-isotropic about the ion path by changing the shape of the holes in the cavities, say from a circular hole to a slot. For the circular hole through the cavity walls the off-axis force is approximately equal to



$$F = -\frac{1}{2} e r \frac{\partial \epsilon_L}{\partial L} .$$

For the long slot the corresponding forces are



$$F_x = -e x \frac{\partial \epsilon_L}{\partial L}$$

$$F_y = 0, \text{ (parallel to slot) .}$$

It can be shown that the deviation of an ion in crossing a gap of the long slot type is <sup>(5)</sup>

$$\sigma = -\frac{e V_0}{T} (\sin \phi) 2\pi f_s \frac{z}{v} .$$

The magnitude of this effect can be judged by determining the change in (n) required to compensate for the gap defocusing. This is found from

$$B = -\delta n \frac{B}{r} z ,$$

giving

$$\sigma = +\frac{e}{m_0 \gamma \beta c} \theta_c B_a z \delta n . \quad (26)$$

An alternative way in which the gap forces could be compensated is to cut the ends of the magnet sections at an angle to the radius, thereby inducing end focusing. To a first approximation the deviation caused by an end angle of  $\theta_{\text{end}}$

$$\sigma = \frac{2\pi Z \tan \theta_{\text{end}}}{N L_a} ,$$

and so the effect of circular holes could be corrected by cutting at an angle

$$\tan^{-1} (N e V_0 \sin \phi / 4T) . \quad (27)$$

Except at very low energies this effect is small and could readily be absorbed in the choice of  $n_a$  and  $n_{a+1}$ .

### 5.2. Orbit Tilt

Another term arises from the possible tilt of the orbits to the z-axis. Although this effect could be eliminated by tilting the rf cavities, the magnitudes of the forces involved are sufficiently small as to be readily absorbed by the axial focusing forces. If motion in the z direction is achieved by use of separate magnets (see Section 9), then there is no orbit tilt effect.

### 5.3. Transit Time

The gap factor for an SOC, when the rf is operated at N times the cyclotron frequency, is analogous to that for the Wideröe accelerator.

The energy gain per gap crossing is simply

$$\Delta T = eV_0 \cos \phi \left[ \frac{\sin \xi}{\xi} \right] , \quad (28)$$

where  $\phi$  is the phase of the ion at the center of the gap,  $\xi$  is given by

$$\xi = gN/r_a = q \frac{\pi}{2} ,$$

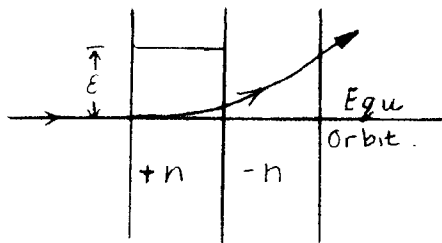
and the gap width is  $2g$ . (It is worth noting that the dependence on  $g$  is considerably less severe here than in an Alvarez-type structure.) In the proposed systems the gaps should not cause any significant reduction in the energy gained per crossing since  $\xi \sim \pi/10$  or less.

## 6. Tolerances

The practicability of any accelerator is intimately tied up with the tolerances on such things as mean magnetic field, the shape of the actual field, the rf voltage amplitude, frequency or phase jitter, and various mechanical misalignments. During the developments of accelerators there has been a steady increase in technology relating to high accuracy magnetic fields and rf voltage amplitude stabilization.

The discussion on field errors in Paragraph 3.2 is extended here; the effect of a simple displacement of part of an otherwise perfect magnet system is examined briefly and simply.

### 6.1. Single Cell Error



Considering the simple displacement of one cell, length  $L_c$ , by an amount  $\epsilon$ , as indicated in the diagram, then the  $z$  and  $z'$  at the end of the following cell are

$$z = \epsilon [ (1 - \cos x) \cosh x + \sin x \sinh x ] \quad (29)$$

$$z' = 2\pi \frac{\epsilon}{L_0} [ (1 - \cos x) \sinh x + \sin x \cosh x ] \quad (30)$$

where

$$x = 2\pi L_c / L_0 ,$$

and  $L_0$  is the wavelength of an oscillation in a (+n) field alone. The value of  $L_0$  is given by

$$L_0 = 2\pi/K,$$

where

$$K^2 = \frac{e}{m\beta c} \frac{dB}{dz} .$$

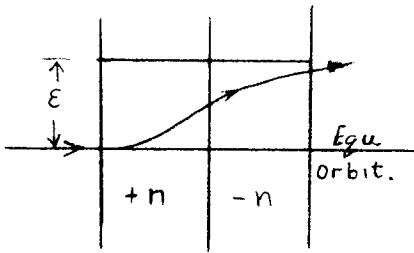
A more direct form is

$$L_0 = 220 \sqrt{\beta\gamma / \frac{dB}{dz}} , \text{ in in.}$$

if  $dB/dz$  is in kG/in.

## 6.2. Double Cell Error

Next consider the error amplitude caused by displacement of a (+n, -n) magnet pair. It is apparent that movement of the magnets in pairs, each pair accurately adjusted within themselves, would reduce the beam disturbance for two reasons. First, there are only half as many 'elements' to be out of line and, secondly, a (+, -) pair induces less oscillation than a single (+n) section having the same  $|n|$ ,  $\epsilon$ , and  $L_a$  values.



The  $z$ ,  $z'$  values at the end of the (-n) cell are

$$z = \epsilon (1 - \cos x \cosh x + \sin x \sinh x) \quad (31)$$

$$z' = \frac{2\pi \epsilon}{L_0} (\sin x \cosh x - \cos x \sinh x) \quad (32)$$

It is apparent that the error caused by displacement of a single (+n) cell is greater than that for a (+, -) pair, at least under the conditions examined. This excess in both  $z$  and  $z'$  increases with  $\epsilon$  and  $x$ , varying as

$$(z_+ - z_{+,-}) = \epsilon (\cosh x - 1), \text{ and}$$

$$(z'_+ - z'_{+,-}) = \frac{\epsilon 2\pi}{L_0} \sinh x .$$

Some indication as to the amplitude of the ensuing oscillation can be found by matching ( $z$ ,  $z'$ ) to a simple sinusoid and computing the amplitude of motion,  $z_m$ , by assuming that the subsequent motion takes place in an undisturbed field system. The wavelength,  $L_v$ , of the ensuing betatron oscillation is found from  $\nu$  and the orbit circumference. The approximate amplitude of oscillation is then found from

$$z_m^2 = z^2 + \left( z' \frac{L_v}{2\pi} \right)^2 . \quad (33)$$

This calculation is only approximate since all straight sections have been omitted. However, for the present case it indicates that  $z_m \sim \epsilon$ .  
 [  $B' = 2kG/in.$ ,  $n = 180$ ,  $L_e = 22.5 in.$ ,  $L_o = 190 in.$ ,  $x = 0.74$  radians,  $\Psi = 0.84$  radians,  $N = 50$ ,  $\cos \sigma = 0.92$ ,  $\sigma = 23^\circ$ ,  $\nu = 3.2$ ,  $L_\nu = 700 in.$  → 31 cells,  $z_m = 1.17$  ].

If it is assumed that the cells are adjusted in pairs and that no programed tuning is performed, then the permissible random error in adjustment is approximately given by

$$X \sim F \epsilon_{rms} \sqrt{\text{No. of pairs.}} \quad (34)$$

where  $X$  is the beam amplitude growth and  $F$  is given by  $z_m / \epsilon$ .

$$[ X = 1/2 in., F = 1.2, \text{No. of cells} = 3,000, \epsilon = 7.6 \cdot 10^{-3} in. ]$$

The minimizing influence of adiabatic damping of betatron oscillations has been omitted in this simple discussion.

### 6.3. Smooth Errors

The preceding discussion indicates that the cell-to-cell displacement errors should be held down to less than 0.01 inch. So far, however, the permissible extent to which the mean orbit can depart from the ideal path has not been determined. Consider the case where  $\epsilon < 0.01 in.$  at each gap but the errors are accumulative, then the actual path could oscillate about the ideal with an amplitude of

$$z_m = \frac{z'_{max} \lambda_e}{2\pi}$$

where  $\lambda_e$  is the wavelength of the error term about the ideal path. Substituting for  $z'_{max}$ ,

$$z'_{max} = N \epsilon / 2\pi r$$

gives

$$z_m \sim \frac{N \epsilon \lambda_e}{4\pi^2 r} \quad (35)$$

If  $N = 50$ ,  $\lambda_e = 2\pi r$ ,  $\epsilon = 0.01$  in., then  $z_m \sim 0.1$  in. This seems to agree with the observation that a 'smooth' error of  $\sim 1/8$  in. in an AGS could be tolerated.

The inference is that the magnets should be aligned by going from cell to cell rather than trying to obtain an absolute, that is, spatial accuracy.

#### 6.4. Mean Field and Frequency Errors

A uniform reduction in the strength of the magnetic field causes the phase-stable angle to become smaller, that is, more towards the crest of the rf waveform, provided the frequency of the rf is unchanged. This is attended by an outwards movement of the equilibrium orbit.

The tolerance on the rf frequency is not clearly definable; the cavity Q sets a pass-band of usable amplitudes, the power amplifier delivers the frequency fed to it from the standard oscillator, and the phase-frequency tuning controls adjust the cavities onto tune.

Because of the square law dependence of the power losses in the cavities upon the phase-stable angle for a given rate of energy gain, the phase-stable angle would be chosen to be relatively small, say between  $-30^\circ$  and  $-20^\circ$ . In consequence, the amplitude of rf voltage should be regulated to within about  $-2\%$  to  $+5\%$ .

## 7. The RF System

A suitable form for the rf system became apparent as a result of studies made in connection with the Mc<sup>2</sup> Cyclotron.<sup>(6)</sup> The basic requirements for a usable system are a high unloaded Q, capability of being designed to operate over a range of frequencies, and not too much sensitivity to asymmetries of design. The conditions are well met by the cavity arrangement shown in Fig. 4.

Although it is possible to consider the entire rf system as part of one extremely large cavity, snaking its way alternately up and down the radial spaces between the magnet sectors, encompassing the entire ring, it is probably not the best solution. The major disadvantage is that the modes which can be supported crowd close together if the cavity is many wavelengths long.

A reasonable solution is to make the system out of several identical parts, each of sufficient size to be driven by one power amplifier tube. The separate cavities could then be correctly phased by control of the amplifier stages.

If it is assumed that a cavity system can be designed, then the power losses for given gap voltages and why the system is more efficient in the conversion of power than a linac are of interest. The power losses to the walls in a cavity of the type shown in Fig. 5 are given by

$$P = \frac{1}{2} (2 d^2 R_s E_0^2) (2 \int_0^{\lambda/4} \cos^2 \beta l dl + d) / z_0^2 . \quad (36)$$

For  $f = 2 \times 10^9$  c/s, [d = 12 in.,  $\lambda = 59$  in., copper walls] this becomes

$$P = (0.065 \times 10^{-5} E_0^2) X \quad (37)$$

where X is the length of cavity per gap.

UNCLASSIFIED  
ORNL-LR-DWG 74888

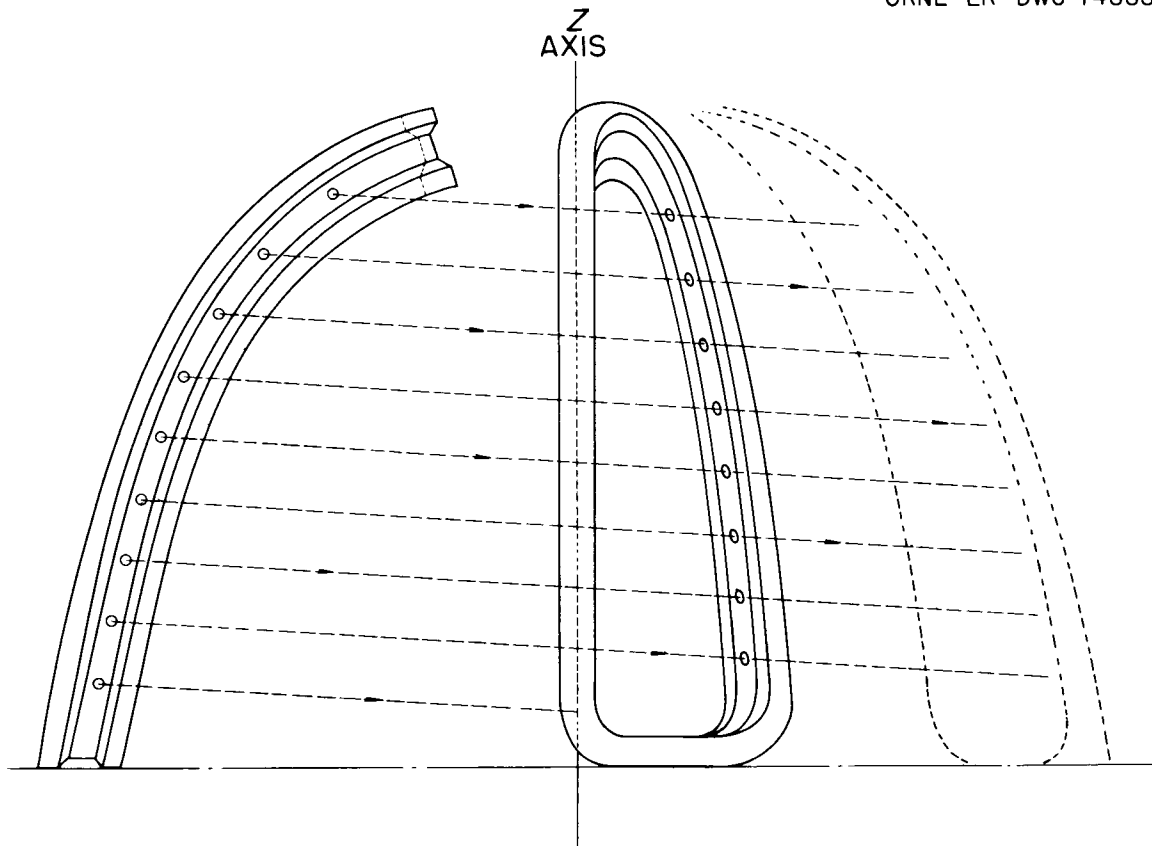


Fig. 4. Sketch of part of suggested radio-frequency cavity system. The electric field is a maximum at the center of the cavity and is parallel to the path of the ions. The separation along the equilibrium orbit between two sets of gaps is simply  $\beta\lambda/2$  where  $\lambda$  is given by  $2\pi mc/NeB_0$  and  $N$  is the number of such cavities.

UNCLASSIFIED  
ORNL-LR-DWG 74710

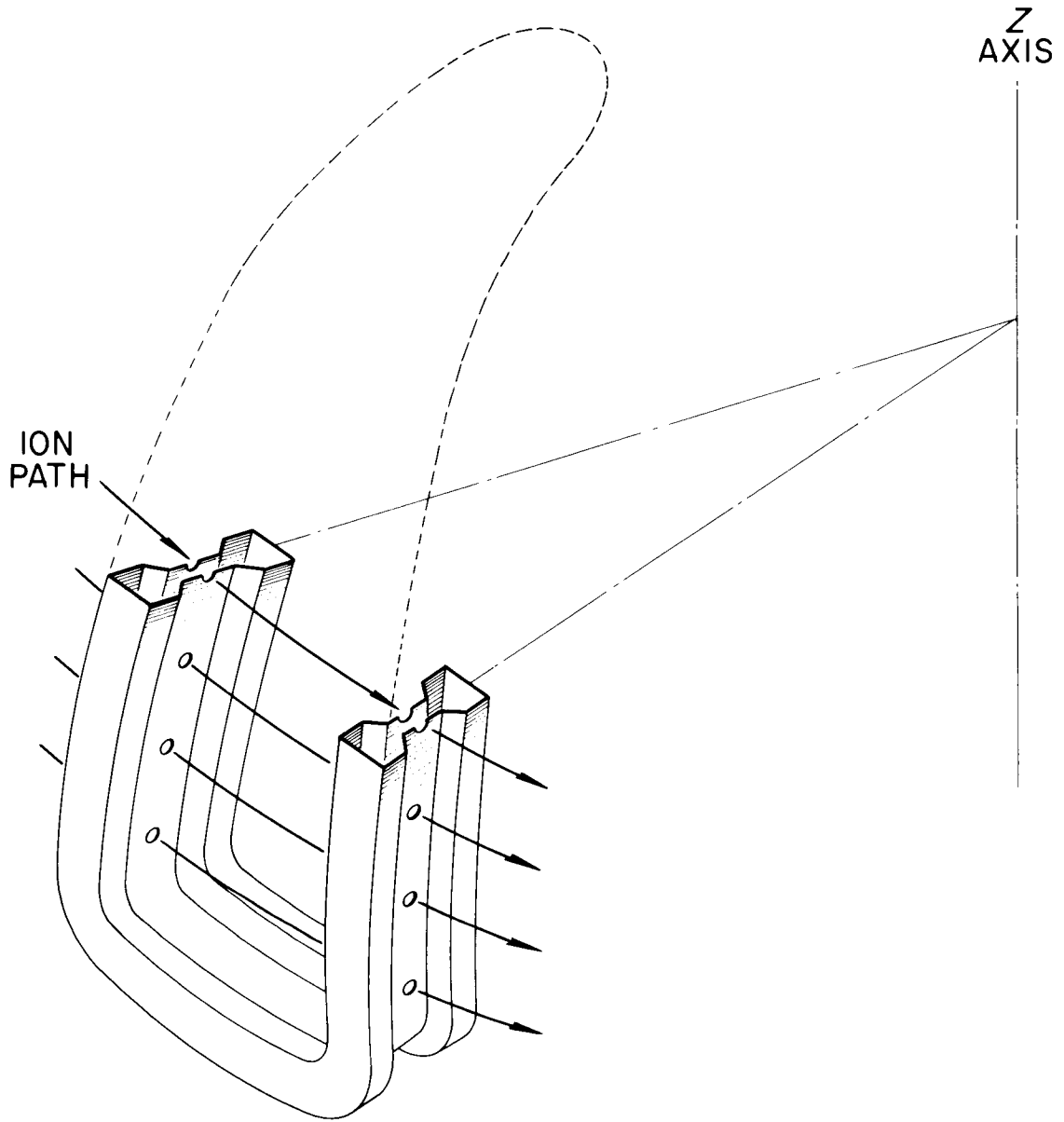


Fig. 5. Artist's sketch of a cavity showing successive passes of the spiraled ion path.

A reduction in the line spacing at the voltage maximum region, so as to permit the insertion of the magnets and reduce transmit line effects, causes an increase in the losses. In the case of a simple step line, as shown in Fig. 6 for example, the dependence of the power losses upon the step ration  $h$  is given in Fig. 7 for the present case; the gap voltage is assumed constant. The total power lost to the walls in a 900-MeV section of machine is thus about 10 Mw.

To compare these values with corresponding values for a linac, the power loss in a simple pill-box cavity with no re-enterant sections is found first. The power is given by

$$P = \pi a R_s E_0^2 J_1^2(ka) (d + a) / 377 \quad (38)$$

where  $(ka)$  is equal to 2.405.

The corresponding expression to Eq. (37) is

$$P = 1.72 \times 10^{-5} E_0^2 \quad (39)$$

Examination of Eqs. (37) and (39) shows that the SOC losses are less severe for two reasons. First, the amount of cavity per acceleration is less and, secondly, the field strength is less. It appears that these two factors are approximately equal in importance in causing an overall reduction in the power losses relative to an equivalent linac. In practice a ten-fold reduction in power level during beam acceleration should easily be obtained.

UNCLASSIFIED  
ORNL-LR-DWG 76870

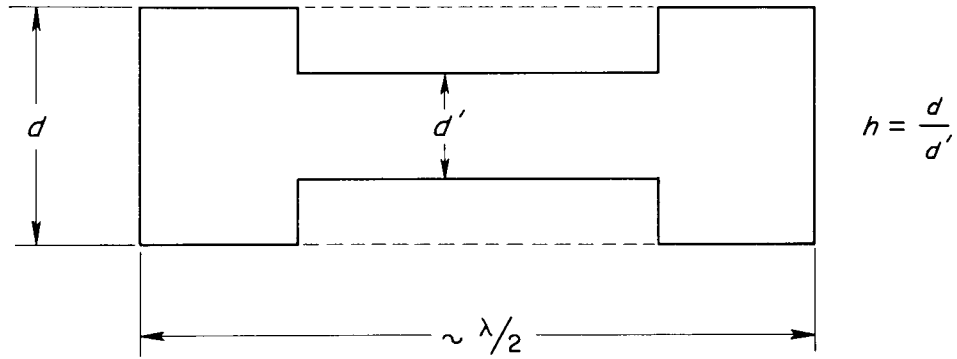


Fig. 6. Cross section of the rf cavity.

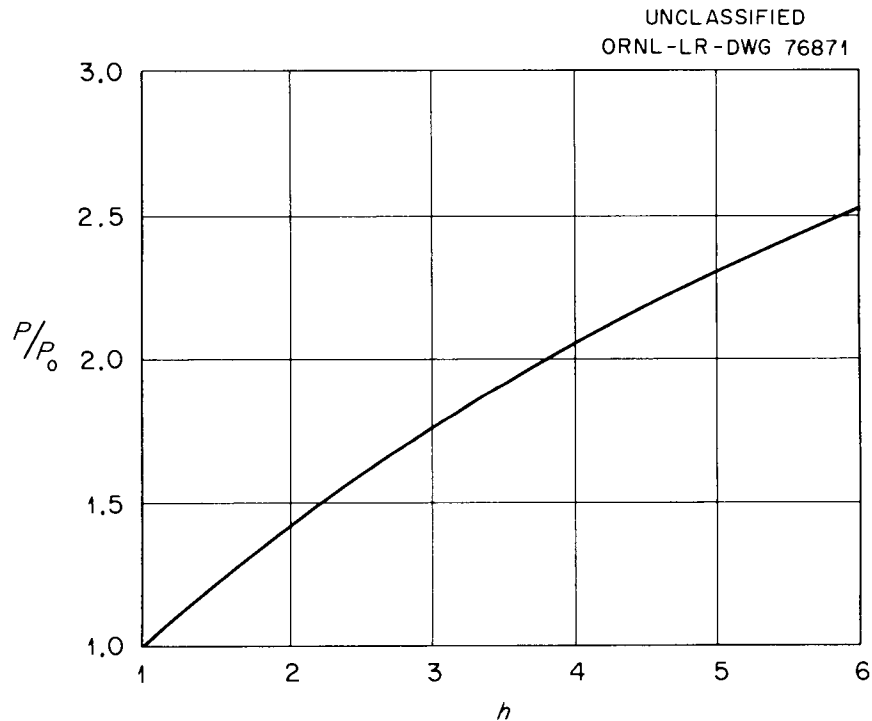


Fig. 7. Plot of the increase in the power dissipated in the rf cavity as a result of decreasing the spacing at the center of the cavity.

## 8. The Magnet

The basic properties of the magnet have already been suggested. An important feature of the stacked arrangement of poles is the high magnetic efficiency which can be obtained. In addition, the several parts forming the magnet are not individually either large or intricate. It is possible that the magnet be constructed from  $N$  sections of identical magnet blocks, the variations required in passing from cell to cell being absorbed in adjustable pole tips. Certainly, at the high-energy end this would be true. However, at low energies it might be necessary to vary the main magnet blocks to make some allowance for the rapidly changing orbit radius.

From the discussion on tolerances it would seem desirable to combine the cells into rigidly connected  $(+n, -n)$  pairs, in conjunction with the rf cavity system. The magnet and rf system might then consist of  $N$  parts as shown in Fig. 8.

The magnitudes of field gradients called for in the design, namely  $2 \sim 3$  kG/in. centered on 5 kG, do not appear to present any major difficulties. Each magnet stack would be terminated at both top and bottom by an extra energizing coil, thus providing the necessary magnetic images for elimination of end-effects.

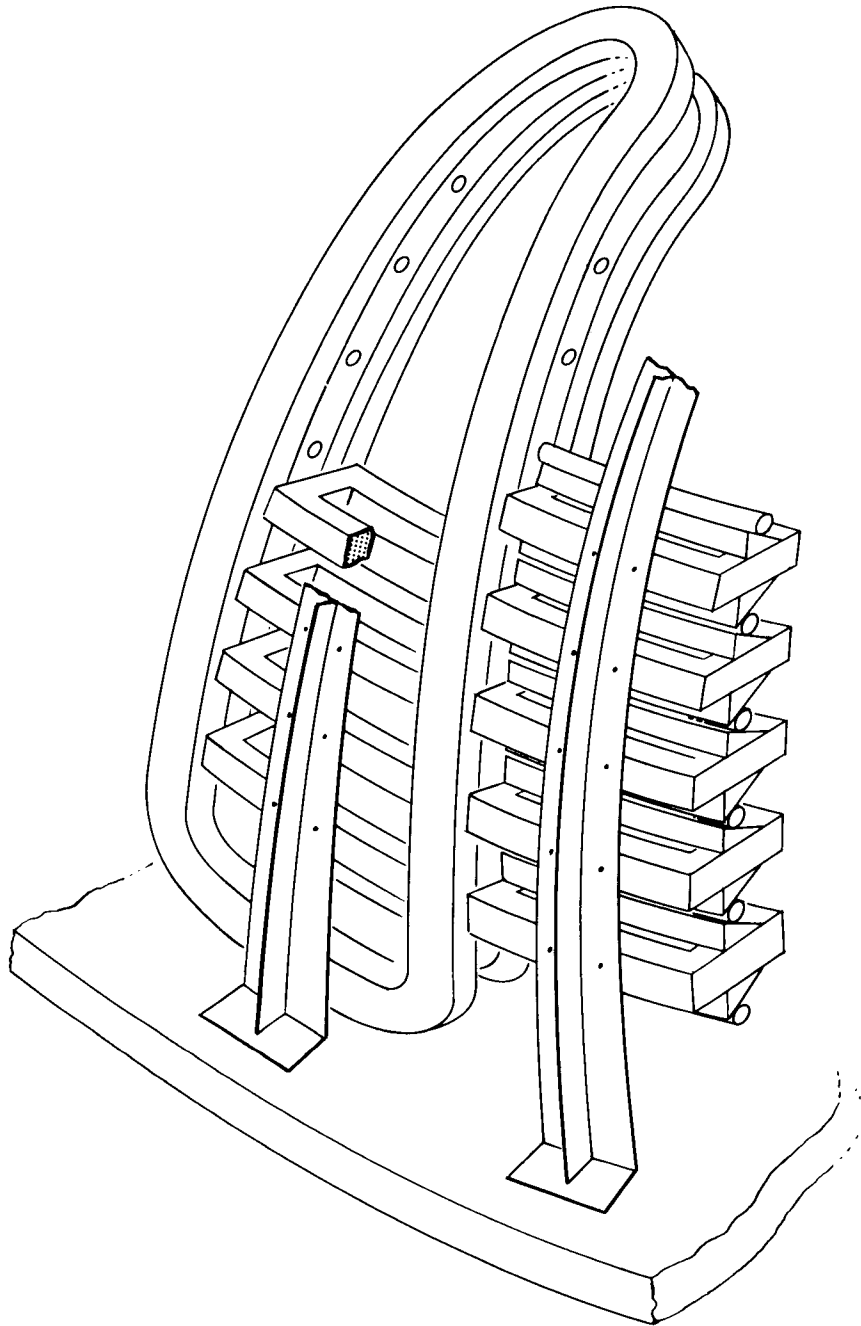


Fig. 8. Sketch of a complete magnet and rf cavity sector. Each sector contains one rf cavity and pairs of magnet cells, the positive and negative gradient sections being mounted upon a common support so that the magnet pairs can be aligned accurately.

## 9. Logical Developments

So far, only the ideal or simple SOC system has been considered. Considerable modification of the basic design appears to be possible without sacrificing too much, so that substantial reductions in both magnet and rf power might be obtained.

Consider the change whereby the ion path is grouped into pairs of turns, each magnet block supporting two pole tips at different radii, and the rf cavity being pierced by two holes at each step in the z direction. A direct result is a reduction by almost two in the magnet power. The features of individual paths which are separately adjustable and accessible are still valid.

To facilitate passage from one turn-pair to the next, requiring both a change in radius and z-dimension, it would be desirable to introduce straight sections around the machine, as is illustrated in Fig. 9. These sections could be of service in other ways; for example, extraction could easily be performed and the beam could be tailored for passage to the next stage in the machine by use of multipole elements. Under these conditions it would no longer be necessary to tilt the ion path along the entire length, the magnet blocks all being perpendicular to the z-axis. A particularly elegant way to construct the magnet for transferring ions from one layer to the next has been suggested<sup>\*</sup>; it is developed later in Section 13 (see Fig. 25).

It should be noted that another consequence of the above change is a reduction in the total height of the machine, resulting in a more rigid structure. The degree of magnetic coupling between the turn-pairs is important and should, ideally, be low.

---

\*E. D. Hudson, Electronuclear Division, Oak Ridge National Laboratory.

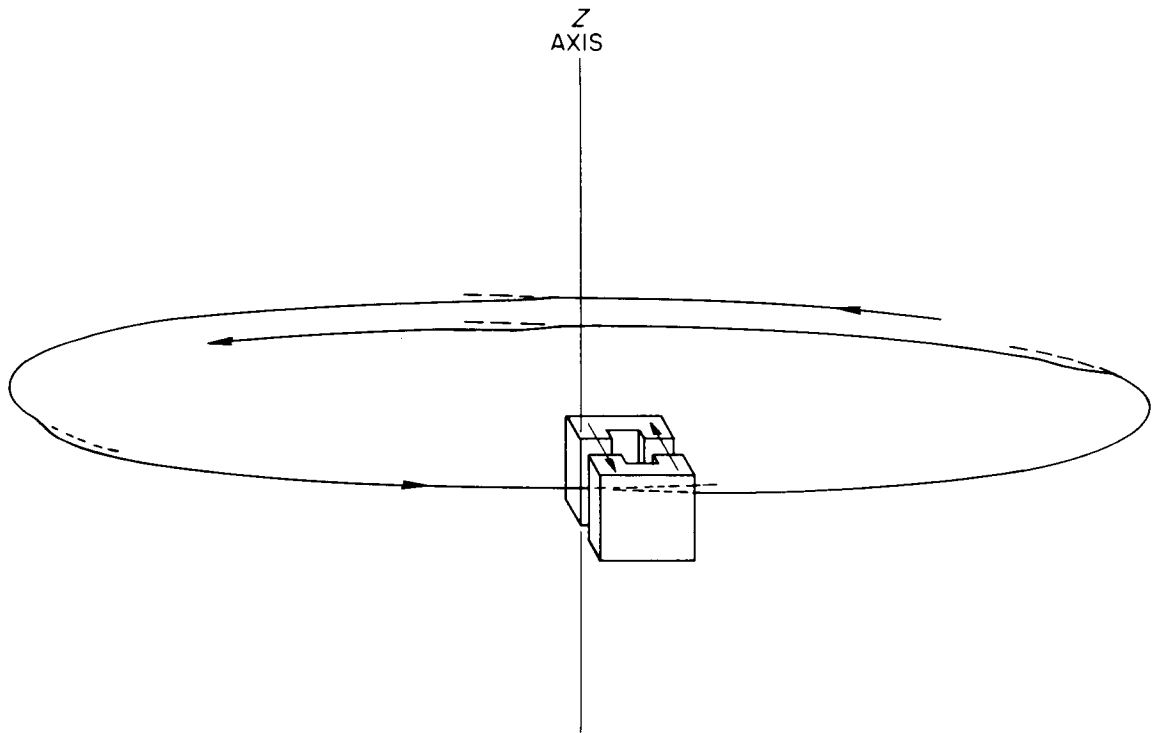
UNCLASSIFIED  
ORNL-LR-DWG 76876

Fig. 9. Vertical bending magnets could be introduced to step the ion path down in the z-direction. The sections of the magnets lying between the bending magnets are thus in the horizontal plane.

## 10. Tune-Up Procedure

The major sequence of adjustments relate to the several thousand pairs of pole-face shims. On the basis of good decoupling between adjacent turns it should be possible to initially assemble and magnetically adjust all shims to within the limits commensurate with successful beam passage.

Subsequently, by means of suitably placed beam position indicators and a "mechanical monkey" the magnetic field could be tuned up either by trial and error, as has been done several times on AVF cyclotrons, or better, by use of computer controlled programs. A preliminary examination of this method indicates that a 1-GeV machine might be optimized in less than one day using a "mechanical monkey" with computer control. Once adjusted, such a machine should remain in tune for a considerable period of time, perhaps indefinitely.

## 11. Applications

In deciding upon applications for an SOC-type of machine it is natural to emphasize the desirable characteristics and to exploit them to within reasonable limits. In review, an SOC exhibits the following properties:

- (a) Continuous output, as from an FF cyclotron
- (b) Transverse stability by strong focusing
- (c) Phase stable in longitudinal motion
- (d) Whole-beam extraction
- (e) Output energy can be varied, as in a linac

Briefly, then, the SOC bears a close resemblance to a continuous working linac in respect to beam quality, size, intensity, and distribution in time. However, it differs markedly in the size and shape of the building housing the machine and in the amount of rf power dissipated in the cavities. These conclusions are still valid even if one considers a superconducting linac, provided that similar arguments are applied to a superconducting rf system, and perhaps magnet, for the SOC.

Consequently, such a machine is well suited to be used either as a meson factory or as an injector to a second accelerator, or both if the second machine is operated in a pulsed manner.

Considering higher energies, obtained by feeding one SOC into another, then a continuous working machine with output energy in the 5 to 15-GeV region is not unthinkable. (A 7-GeV machine, having 1,000 to 3,000 times larger beam current than a proton synchrotron of similar energy, would cost about five times as much.) Such a machine might be called an 'anti-proton-factory'.

In Fig. 10 a shaded area representing the potential performance range of the SO cyclotron is superposed on an earlier figure<sup>(7)</sup> representing the areas of performance of the various types of existing accelerators.

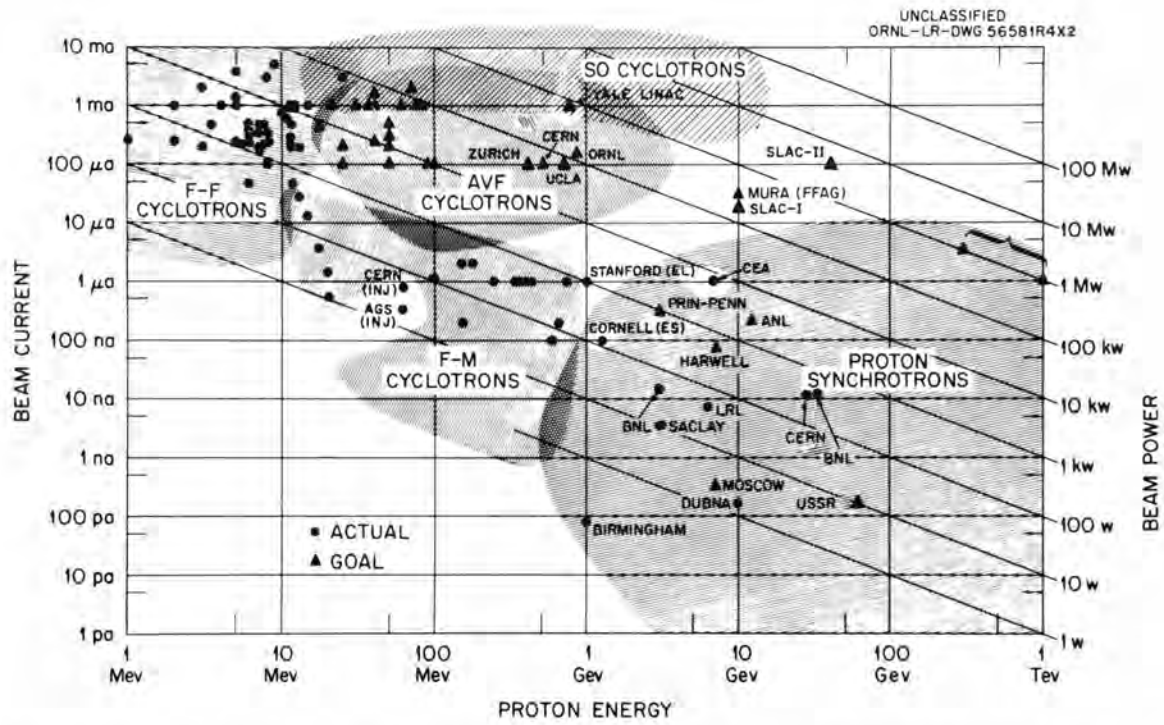


Fig. 10. Potential performance range of SO cyclotrons compared with the ranges of other types of existing accelerators.

## 12. Design of a 1-GeV Machine

In this simplified initial design little attempt will be made at refinement; only the basic SOC concept will be used. Where possible relevant experimental results will be given to support design numbers. A more detailed description of a proposed machine, indicating the lines of development, will be given in Section 13.

A more efficient accelerator system can be designed by separating the machine into several parts: the injector, intermediate section, and the final stage. Each part can then be designed for optimum operating conditions, as indicated in Table I. The range of energy best covered by a particular type is not fixed definitively: this is especially true of the first change (from a linac to a SOC). It is assumed that a continuous working linac can be designed to fulfill the injector requirements of about 1.0 to 10 mA mean current at 15-MeV energy.

Table I. Components of an Accelerator System for 1-GeV Protons

	<u>Energy Range</u>			<u>Type</u>
1.	0	-	0.5 MeV	Cockcroft-Walton
2.	0.5	-	15 MeV	Continuous working linac
3.	15	-	120 MeV	1st SOC
4.	120	-	1,000 MeV	2nd SOC

### 12.1. The 120-1,000 MeV SOC, Basic Design

Since the major part of the machine is the last stage, it is logical to start with that section, thereby fixing many of the parameters for the other sections.

Magnet. -- To simplify the design, it is assumed that  $v_z \approx v_r$  and that a simple spiral helix orbit path is used. Critical dimensions of the magnet are indicated in Fig. 11 and the chief parameters are given in Table II.

UNCLASSIFIED  
ORNL-LR-DWG 76873

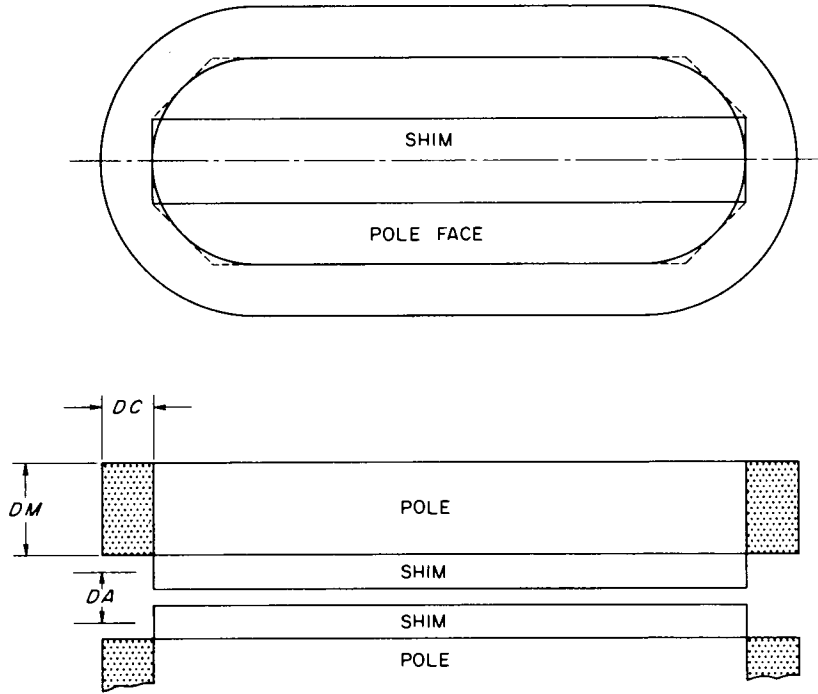


Fig. 11. Diagram indicating the magnet dimensions.

UNCLASSIFIED  
ORNL-LR-DWG 76874

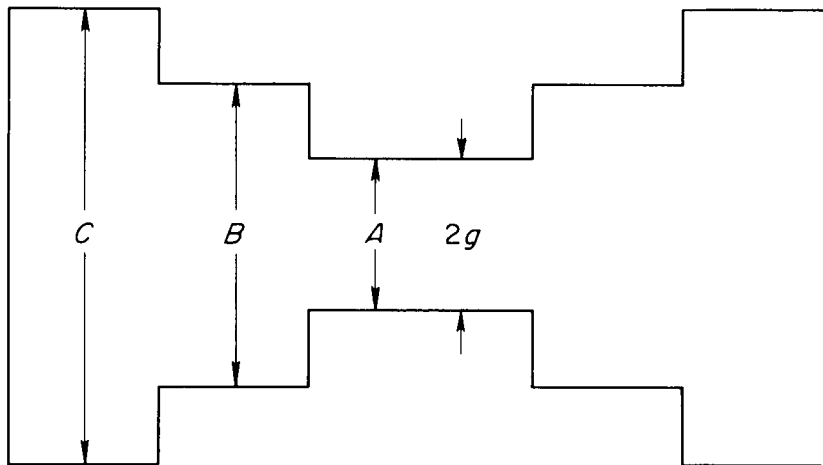


Fig. 12. Cross section of the rf cavity, showing the changes in the wall spacing.



The Radio-Frequency System. -- The acceleration system is assumed to consist of 50 identical cavities, each phased with respect to the others. A constant gap (2g) has been assumed to simplify the power calculations. Operation is at the N'th harmonic of the cyclotron frequency. The properties of the cavities are described in Table III.

Table III. Properties of RF System

$f_o$ , cyclotron frequency (Mc/s)	3.42
$f_r$ , frequency in cavities (Mc/s)	170
Total number of accelerations, in 60 turns	6,000
Energy gain, mean (keV/gap)	147
Power loss of cavity (kW/ft)	4.6
Cavity spacings, see Fig. 11	
2g (in.)	3.0
A (in.)	3.0
B (in.)	6.0
C (in.)	12.0
Length of each cavity (ft)	61
Electric field strength in cavity (kV/in.)	50
Total power loss to cavities at $\phi_s = 0^\circ$ (MW)	15.1
Total power loss to cavities at $\phi_s = 20^\circ$ (MW)	16.1
Beam loading at 1 mA, mean (MW)	0.88
Beam loading at 10 mA, mean (MW)	8.8
Surface area of cavities, total (ft <sup>2</sup> )	$20.5 \times 10^3$

Vacuum System

Volume, beam pipe only (ft <sup>3</sup> )	100
Volume, beam pipe and cavities (ft <sup>3</sup> )	3,000
Vacuum pressure (mm Hg)	$10^{-5}$

Orbit Properties

$\nu_r = \nu_z$	9.2 at 120 MeV,	7.7, at 1,000 MeV
-----------------	-----------------	-------------------

## 12.2 The 15-120 MeV SOC, Basic Design.

In this first-stage SOC it is assumed that the radio frequency is the same as that in the high-energy region, but that the machine is operated in the second harmonic mode. The main reason for this change is to ease the design of the central or low energy part. An alternative procedure would be to double the 'cyclotron radius' used in this section. A plot of the height of the ion path as a function of orbit radius is given in Fig. 13, together with inserts showing magnet details. Properties of the radio-frequency system are summarized in Table IV, below; the magnet is described in Table V.

---

Table IV. Properties of RF System, First-Stage SOC.

---

$f_o$ , cyclotron frequency (Mc/s)	3.42
$f_r$ , frequency in cavities (Mc/s)	170
Total number of accelerations, in 25 turns	1100
Energy gain, mean (keV/gap)	96
Power loss of cavity (kW/ft)	2.35
Cavity spacing	
2 g, at 15 MeV (in. )	2.0
2 g, at 120 MeV (in. )	3.0
Length of each cavity (ft)	35
Total power loss to cavities, at $\phi_s = 0^\circ$ (MW)	1.8
Total power loss to cavities, at $\phi_s = 20^\circ$ (MW)	2.0
Beam loading at 1 mA, mean (MW)	0.105
Beam loading at 10 mA, mean (MW)	1.05
Surface area of cavities, total (ft <sup>2</sup> )	5200

---

### Vacuum System

Total volume (ft <sup>3</sup> )	25
Pressure (mm Hg)	10 <sup>-5</sup>

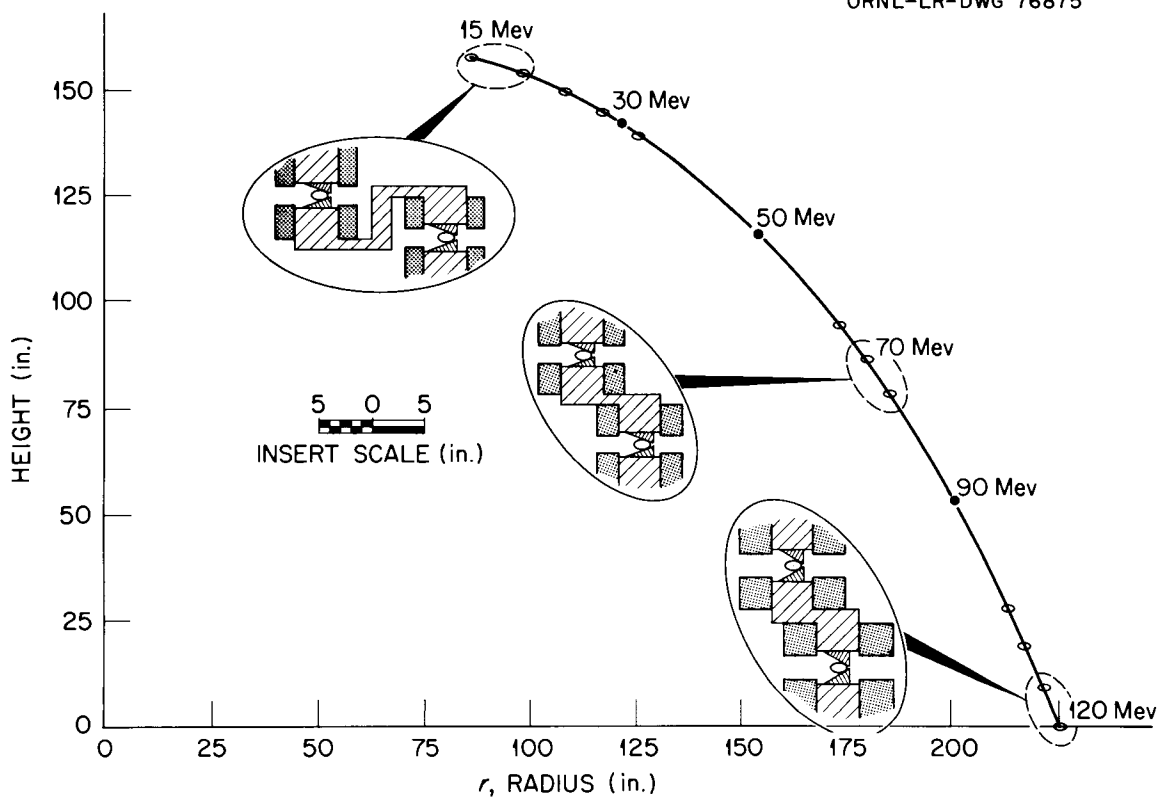
UNCLASSIFIED  
ORNL-LR-DWG 76875

Fig. 13. Plot of ion paths at a given azimuth of the first-stage SOC, with inserts showing magnet details.

Table V. Magnet Parameter for First-Stage SOC, Basic Design

Height (ft)		16
2 N (number of cells/turn)		44
Number of turns		25
$r_o$ , cyclotron unit (in. )		490
$B_o$ (kG)		2.54
	<u>at 15 MeV</u>	<u>at 120 MeV</u>
r (in. )	86.5	226.0
B (kG)	3.64	3.98
Length of ion path (ft)	-	2400
dB/dr (kG/in. )	2.1	2.3
n	50	130
(dB/dr)/B, (in. <sup>-1</sup> )	0.58	0.58
DC (in. )	1.5	3.0
DA (in. )		1.5
Weight of magnet, less shims (tons)		120
Support structure		45
<u>Magnet Coils</u>		
Number, 44 for each of 25 orbital turns		1100
Cross-section area, at 15 MeV (in. <sup>2</sup> )		6
Cross-section area, at 120 MeV (in. <sup>2</sup> )		9
Form factor		0.8
Resistance of ion path, mean (ohm/ft)		$2.7 \times 10^{-6}$
Total power (kW)		627
Power loss, mean (W/ft)		243
Weight of copper, with image coils (tons)		121

### 12.3 Cost Estimate for SOC System, Initial Design.

It is estimated that an accelerator system incorporating the basic SOC concept to provide a 1-mA beam of 1-GeV protons would cost about  $\$18 \times 10^6$ . This is the cost of the complete accelerator system, as summarized in Table VI. It does not include the cost of the building or the experimental facilities, which should be comparable to such costs for other types of accelerators of comparable output.

The author assumes the sole responsibility for the cost estimates given here. In the preparation of these estimates the following assumptions were made:

1. Output - proton beam current 1 mA, mean, at 1 GeV.
2.  $\phi_s$  - at  $20^\circ$ .
3. DC-2 -rf conversion efficiency - at 60%.
4. RF power supply - at \$100/kW.
5. Tubes, 500 kW - at \$45,000 each.
6. Cavities - at \$20/ft<sup>2</sup> worked copper surface.
7. Coils, finished and assembled - at \$3/lb.
8. Magnet pole faces and blocks - at \$0.50/lb.
9. Pole shims, first SOC - at \$40/ft of ion path.
10. Pole shims, second SOC - at \$20/ft.
11. RF parts (circuits, etc) - at \$130/kW.

Table VI. Cost Estimate for 1-GeV SOC, Initial Design

<u>Cockcroft-Walton Injector (0.5 MeV)</u>		$\$250 \times 10^3$
<u>Linac (15 MeV)</u>		
Cavity, drift tubes, etc.	$\$280 \times 10^3$	
Power supply (3 MW for RF)	400	
RF parts	600	
Tubes	200	
Total		$\$1,480 \times 10^3$
<u>First SOC (15-120 MeV)</u>		
Pole shims and adjustments	$\$100 \times 10^3$	
Magnet and support	200	
Coils	600	
Magnet power supply	70	
Cavity	100	
RF parts	300	
Power supply	300	
Tubes	150	
Vacuum and beam pipe	100	
Total		$\$1,920 \times 10^3$
<u>Second SOC (120 MeV - 1 GeV)</u>		
Pole shims and adjustments	$\$250 \times 10^3$	
Magnet and support	550	
Coils	1,300	
Magnet power supply	600	
Cavity	400	
RF parts	2,200	
Power supply	3,000	
Tubes	1,600	
Vacuum and beam pipe	500	
Controls	1,000	
Total		$\$11,400 \times 10^3$
Total cost of complete accelerator system		$\$15 \times 10^6$
Contingency, 20%		3
TOTAL		$\$18 \times 10^6$

### 13. Development of a Proposed SOC

Starting with the basic SOC concept used in the initial system described above a more efficient design is developed for the second or last section of the system. In Fig. 14, curves are given showing the dependence of turn spacing, radius, and number of turns, each as a function of particle energy. A plot of height vs radius of orbit path is shown in Fig. 15 for the basic helical pattern. An obvious difficulty with such an arrangement is the lack of rigidity of the magnet structure, partly caused by the great height of the magnet stacks.

By using pairs of turns at the low energy end, some saving in magnet power and in height of stacks is achieved, along with an increase in rigidity. This is illustrated in Fig. 16. Extending this idea to encompass the entire high-energy SOC results in a much more compact magnet. Considerable saving in magnet power and also in rf power is then possible, the latter occurring primarily because of the reduced length of the cavities. The orbit path in (z-r) space is shown in Fig. 17. A plan view of such an arrangement is given in Fig. 18; two of the four straight sections are indicated. The manner of use of these straight sections is indicated in Fig. 19, showing motion in the z-direction and also crossing of the orbit paths. An obvious difficulty with such an arrangement is that the orbital path lengths at high energy are not exact, being either too large or too small. However, by changing paths, as at point 'C', this defect can essentially be removed.

An alternative line of development now is examined. Instead of using pairs of paths let the helical path be reversed in its z-motion at the half-height point, as illustrated in Fig. 20. By rearrangement of the magnet coils and magnet blocks, a more compact and very rigid structure results, as indicated in Fig. 21. A plan view of this design is given in Fig. 22.

The sudden change in direction of motion along the z-axis, however, introduces some difficulty in the design of a suitable rf cavity. This is overcome by making the change in direction less sudden, allowing several turns to lie in the same plane, as indicated in Fig. 21 by the line of points.

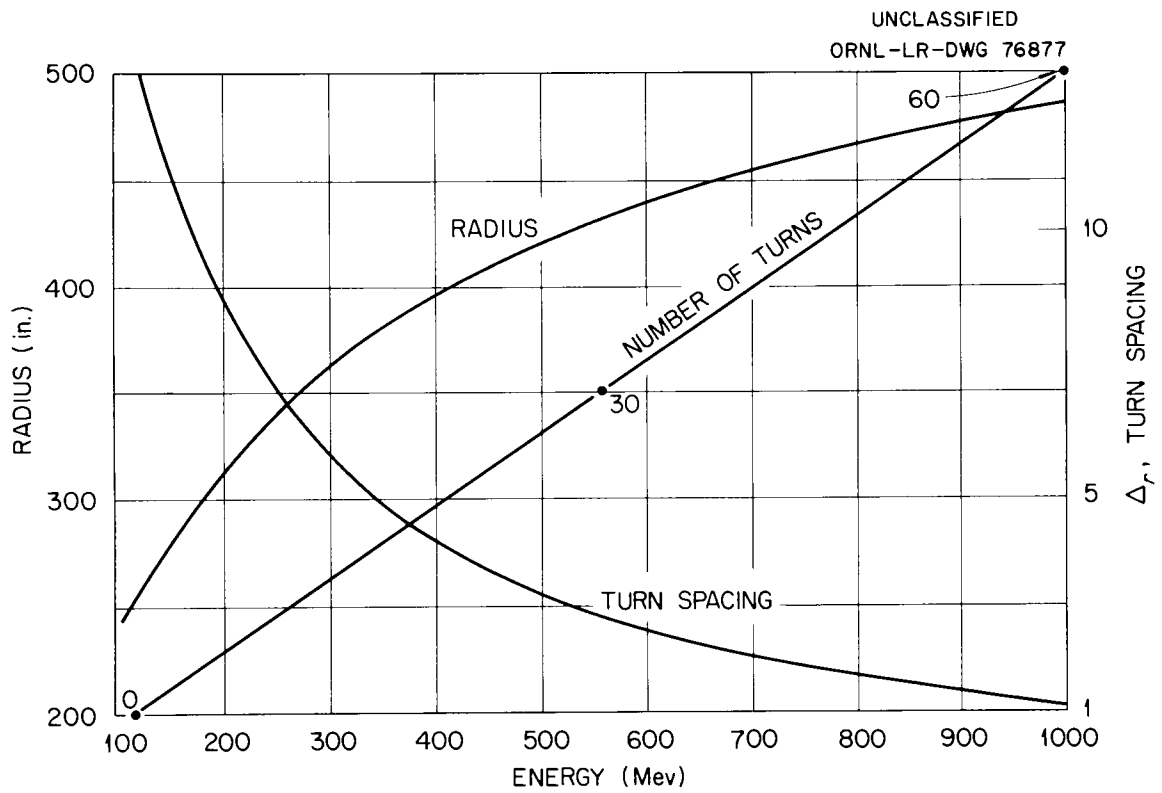


Fig. 14. Turn spacing, orbit radius, and number of turns as functions of particle energy.

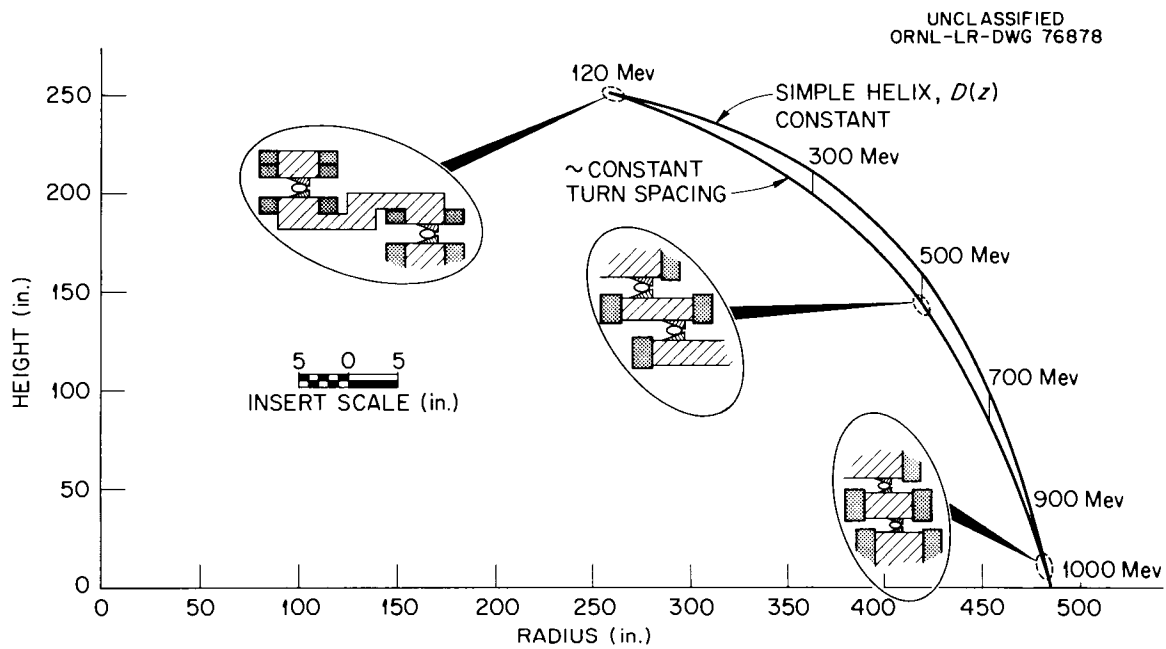


Fig. 15. Azimuthal section showing magnet height versus radius of orbit path, with inserts showing suggested magnet details.

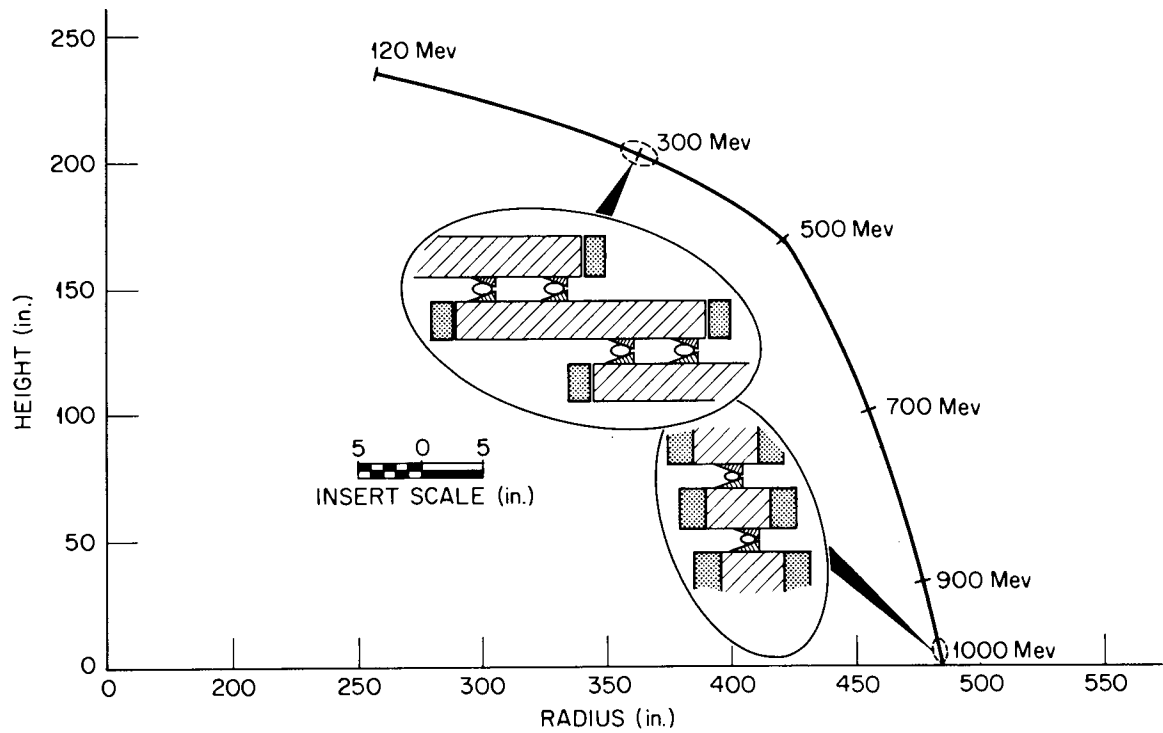
UNCLASSIFIED  
ORNL-LR-DWG 76879

Fig. 16. As Fig. 15 but with paired orbits at lower energy.

UNCLASSIFIED  
ORNL-LR-DWG 76880

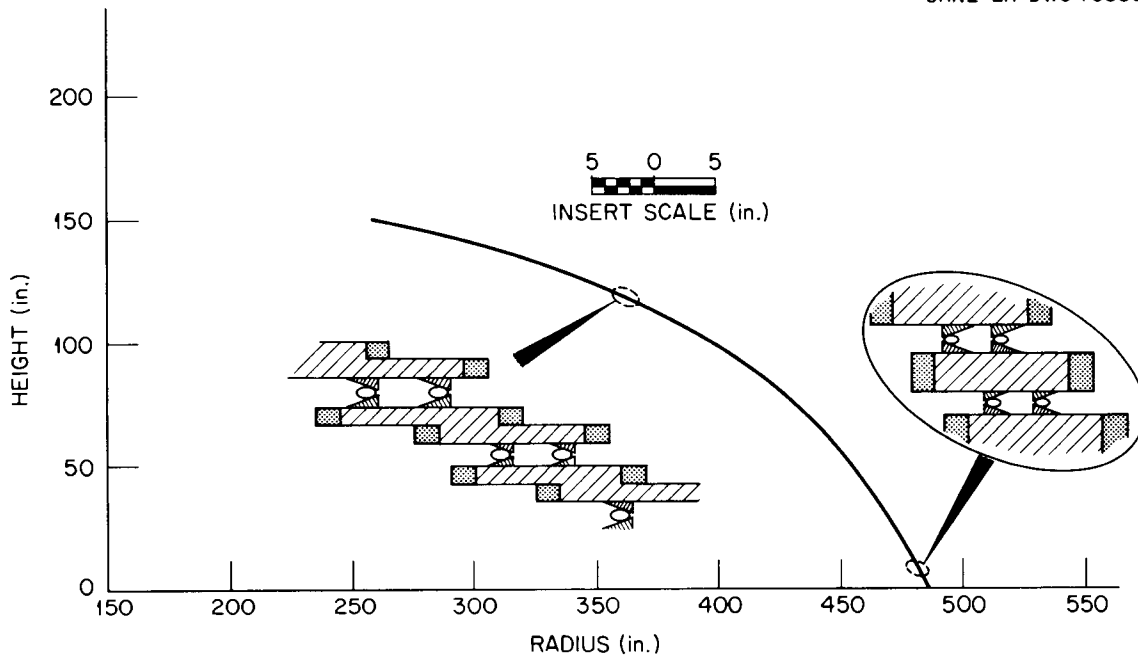


Fig. 17. Compact design with orbits paired at each level.

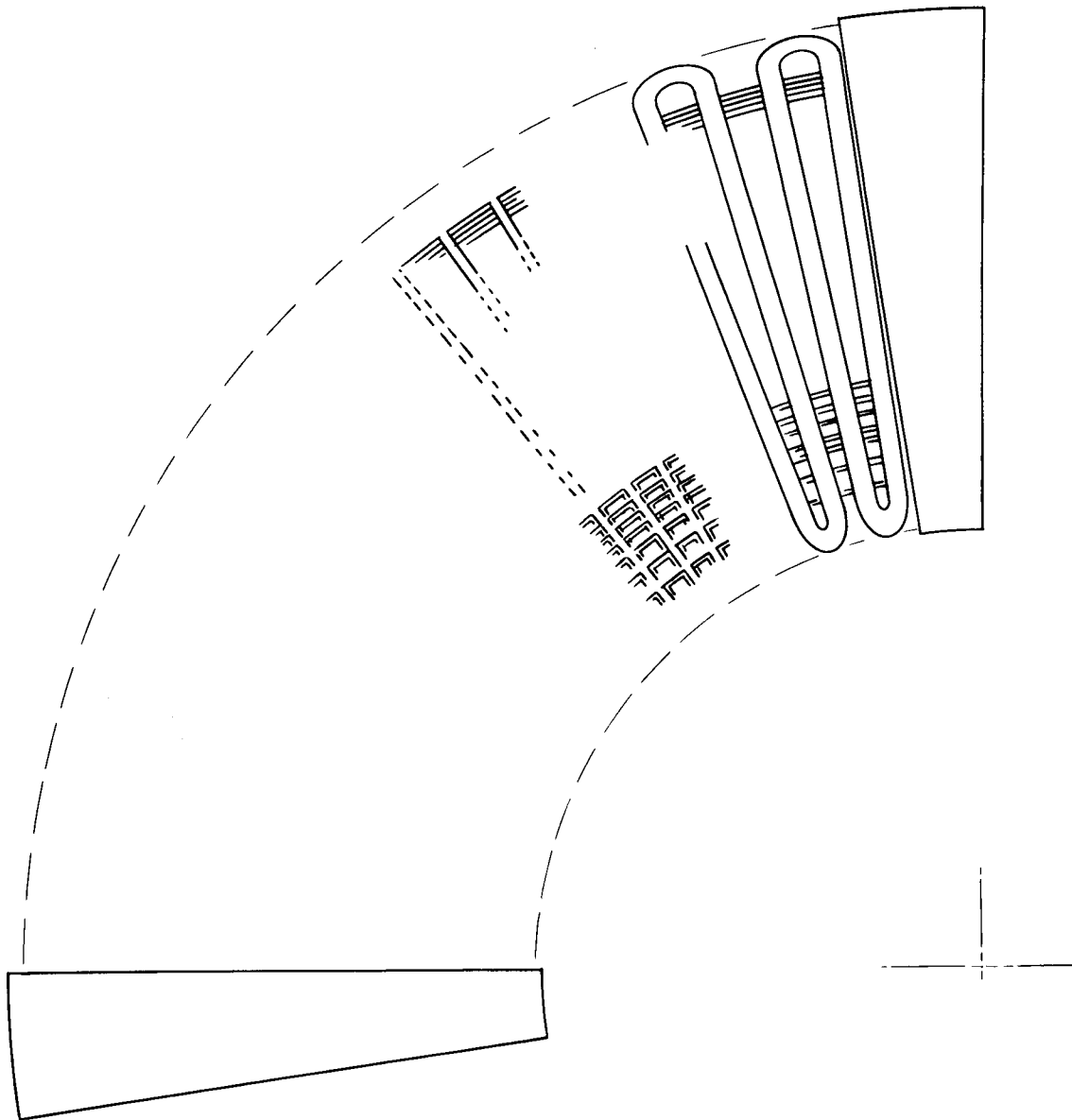
UNCLASSIFIED  
ORNL-LR-DWG 76881

Fig. 18 Plan view of one quadrant of machine showing relative positions of rf cavities and magnet stack. In this instance the magnet coils surround each element of the magnet.

UNCLASSIFIED  
ORNL-LR-DWG 76882

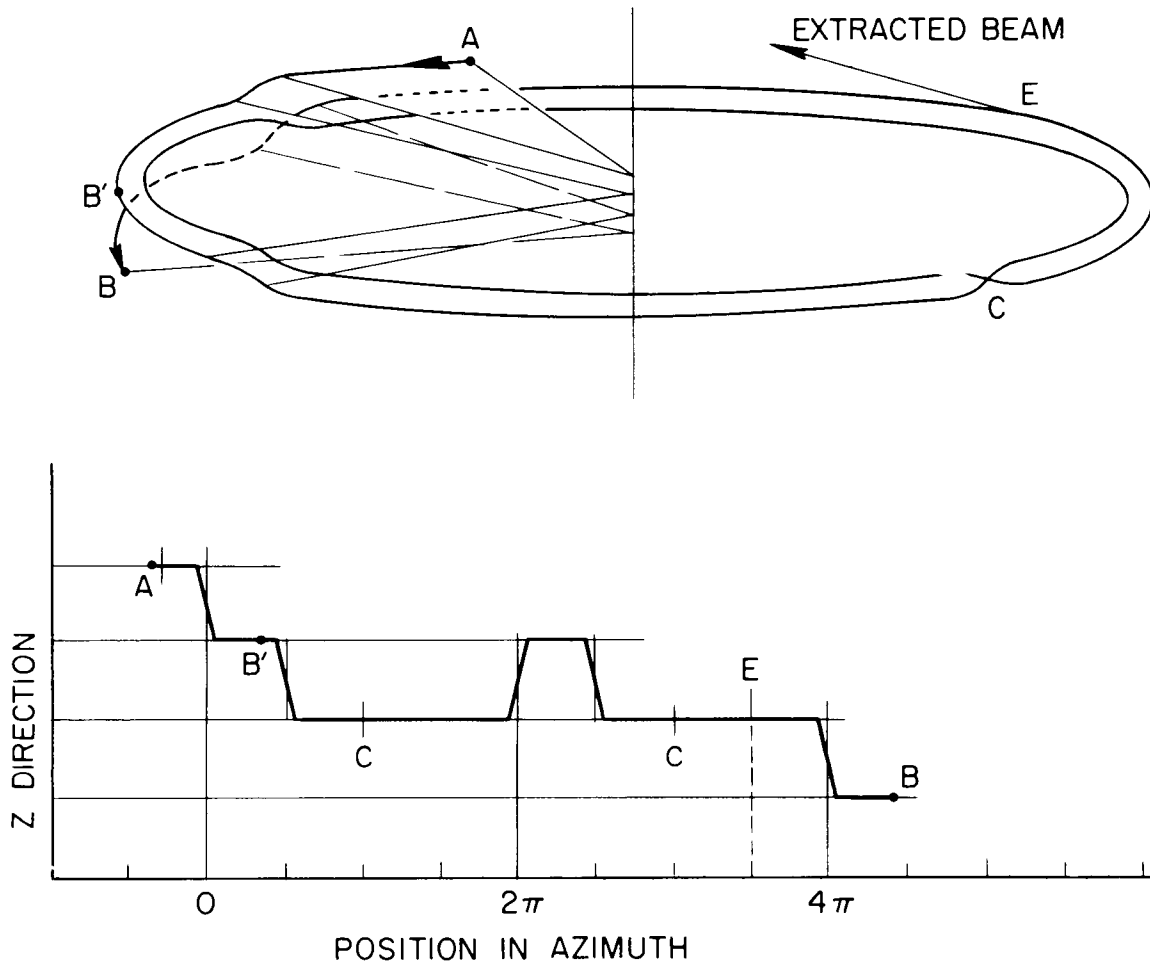


Fig. 19. Upper: Diagram illustrating manner in which orbit paths are changed so as to give the same orbit length for two turns lying effectively, but not actually, in one plane.  
Lower: Plot of Z-motion of ion following the path shown above.

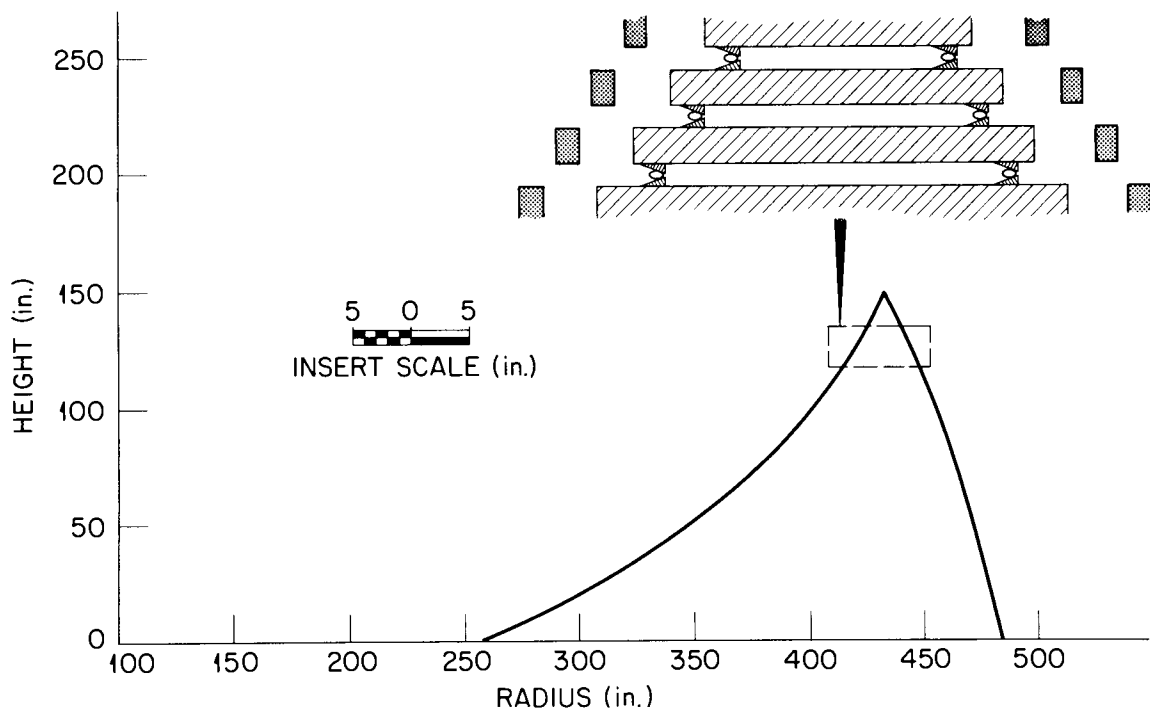
UNCLASSIFIED  
ORNL-LR-DWG 76883

Fig. 20. Magnet design with Z-motion reversed at half-height.

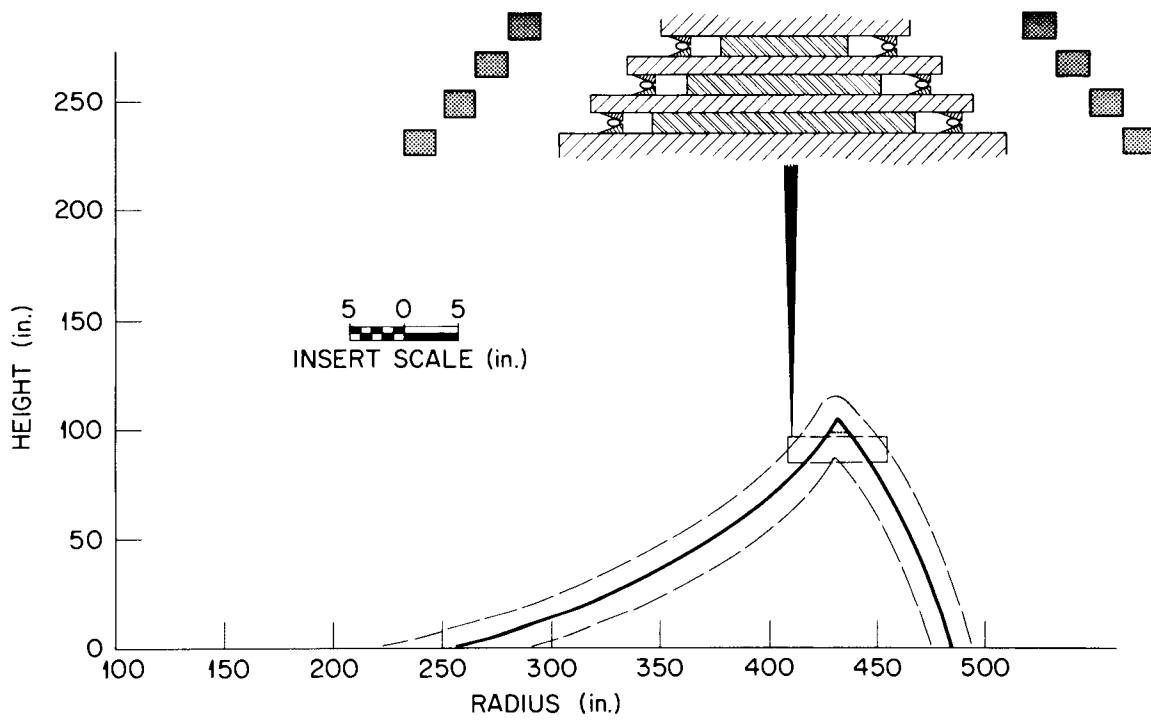
UNCLASSIFIED  
ORNL-LR-DWG 76884

Fig. 21. As Fig. 20 but with magnet stack reduced in thickness and the coils turned on edge.

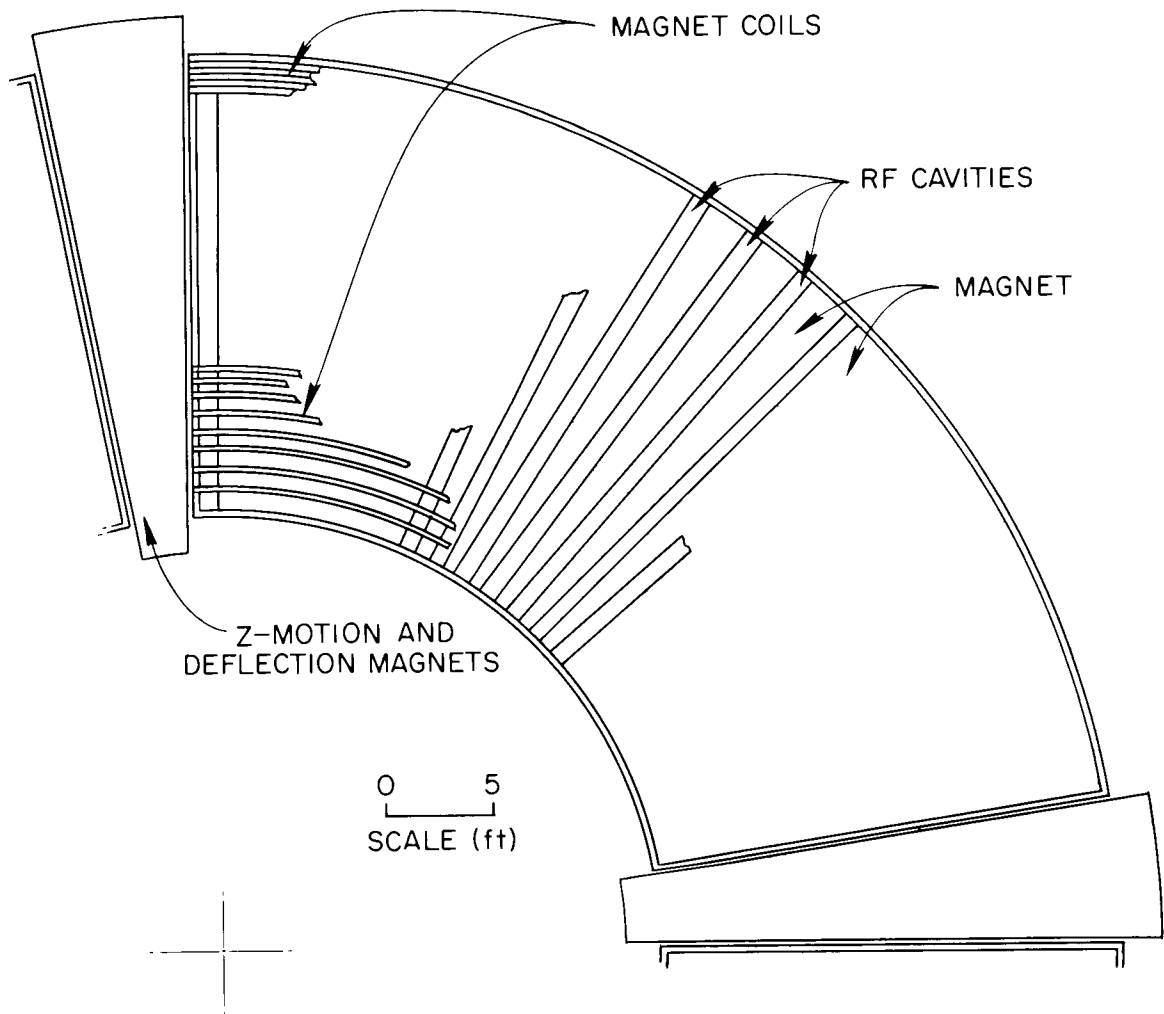
UNCLASSIFIED  
ORNL-LR-DWG 76885

Fig. 22. Plan view of one quadrant of machine. The magnet coils are seen to lie over both the rf cavities and the magnet. Wedge sections are indicated at both ends.

A more detailed section, taken radially, showing possible magnet structure, coils, and rf cavity system is shown in Fig. 23. Some experimental tests which have been made for the magnet geometry indicate its feasibility. Section A-A, shown in Fig. 24, is a cross section through the rf cavity, and Section B-B, shown in Fig. 25, is a plan view detail of the magnet and cavity arrangement.

One of the vertical bending magnets situated in a straight section is illustrated in Fig. 26, and in Fig. 27 a possible extraction magnet and arrangement is shown. With such a system the output energy would be adjustable with an interval of about 20 MeV. An artist's impression of one such machine is given in Fig. 28.

To place the pole shims accurately and to permit them to be adjusted in position, an arrangement such as shown in Fig. 29 and 30 could be used. The basis for this method is that the pairs of shims are accurately located relative to each other. Also, they are maintained accurately within limits on tilt and twist by their position between the pole faces or blanks forming the magnet stack. The only adjustment necessary to 'tune' the machine is, then, the correct radial location of the shim pairs. To facilitate this adjustment, the vacuum tube is constructed with bellows at either end to provide flexibility.

The construction envisaged for the rf cavities takes advantage of the large amount of duplication that is involved in the 2N cavities. It is proposed that the cavities will be built up from small, stamped and formed, sheet copper sections of the type shown in Fig. 31. This type of construction is possible because the joints between sections are parallel to the rf current paths and do not impede current flow.

The sections could be cooled by passing water through passages or corrugations formed into the sheet metal which, besides increasing the rigidity of the structure, reduce the rf skin losses. Approximately 88% of each cavity could be constructed from this basic section, thereby considerably reducing the number of man-hours spent in fabrication.

In addition, two identical end sections and one 'elbow' section are necessary per cavity. Although these parts could be fabricated in the same way as the straight sections the overall cost might be less if the sections are made with cooling pipes welded to developed sheet metal. The outer vacuum vessel for the rf liner is indicated in Fig. 32.

To stabilize the cavities mechanically a tube of either fused silica or alumina might be used as a spacer surrounding each acceleration gap. Finally, to control the phasing and tuning of each cavity a servo-controlled trimmer system could be used.

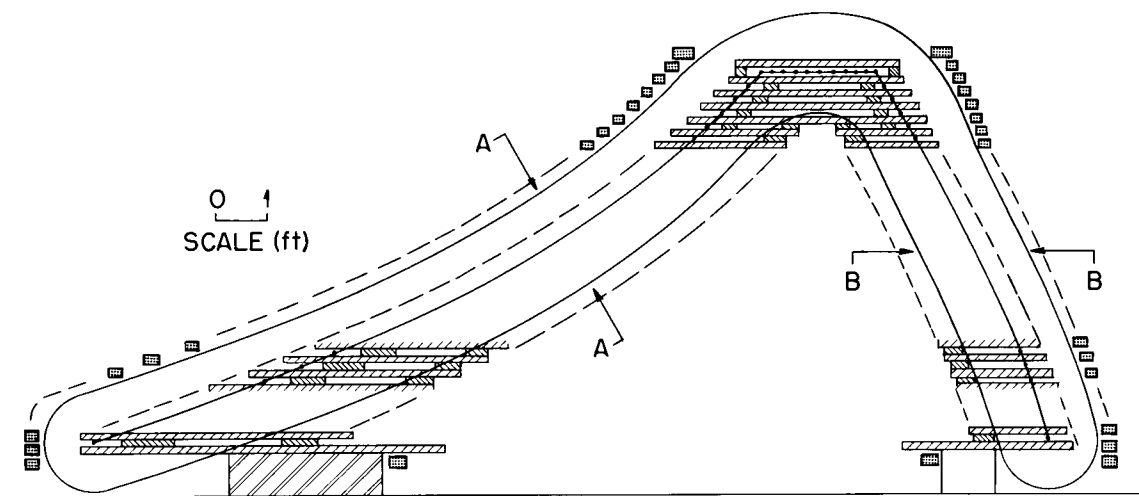
UNCLASSIFIED  
ORNL-LR-DWG 76886

Fig. 23. Radial-cross section of an SOC intended to accelerate protons from 120 MeV up to 1 GeV. A single rf cavity is used and is bent at the mid-energy point. End coils for correcting the magnetic field distribution are indicated at both top and bottom of the coil system. The successive points traversed by the beam are indicated by dots.

UNCLASSIFIED  
ORNL-LR-DWG 76887

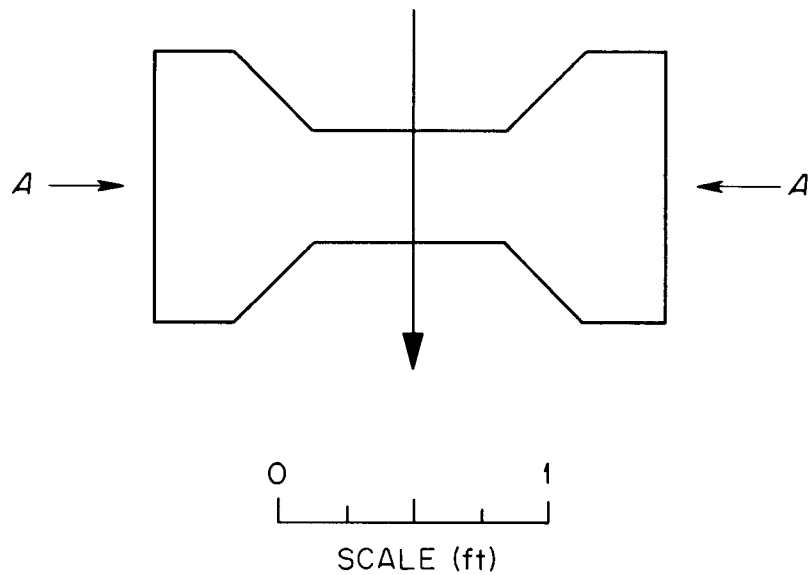


Fig. 24. Cross section A-A of rf cavity showing path of beam and the variation of line spacing to reduce cavity losses.

UNCLASSIFIED  
ORNL-LR-DWG 76888

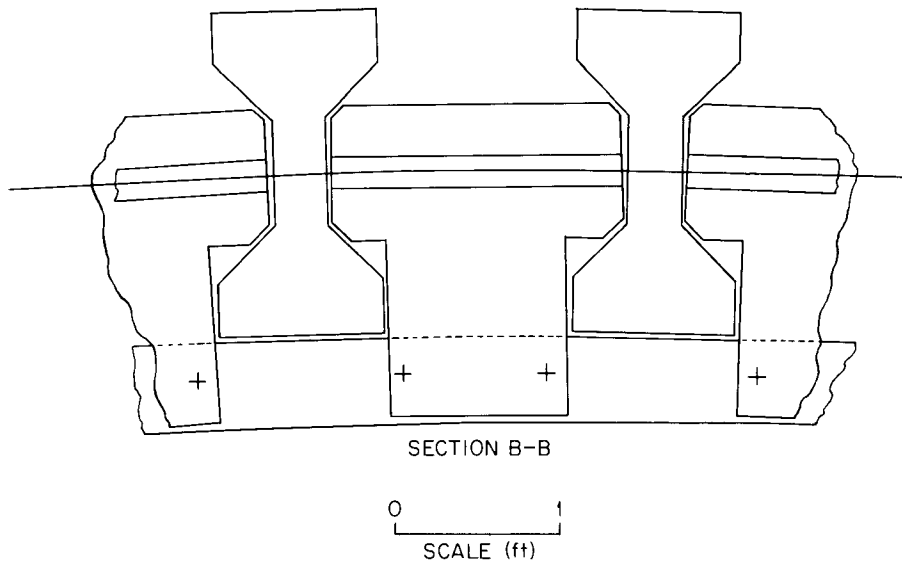


Fig. 25. Cross section B-B of Fig. 22 indicating the relative locations of the rf cavities, magnet stacks, magnet support, and ion path.

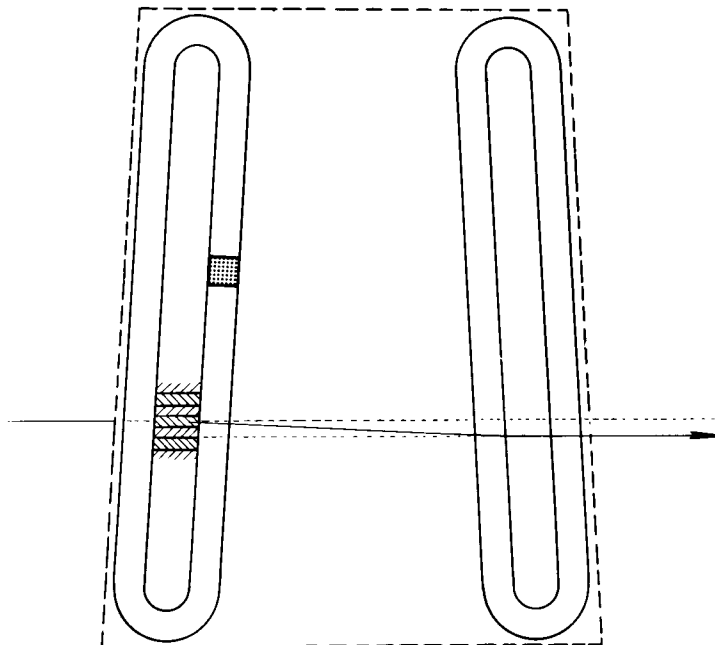
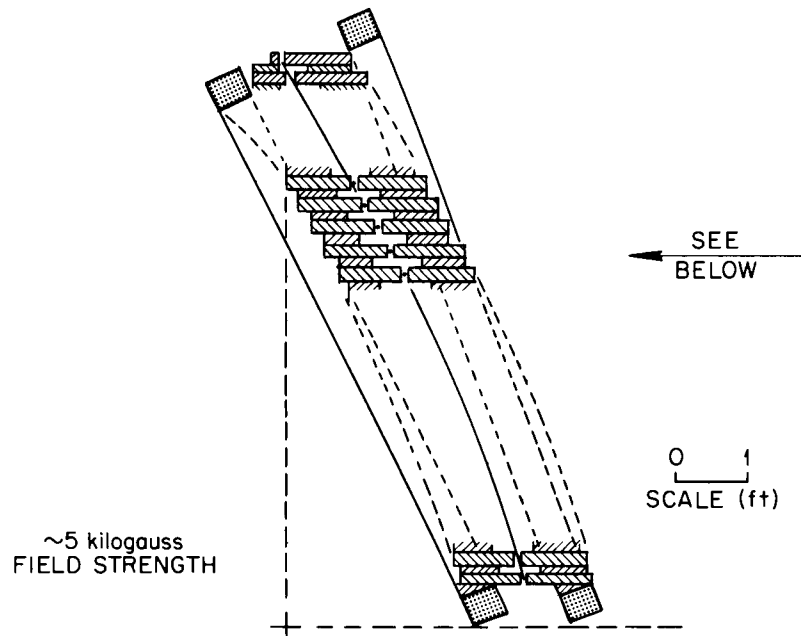
UNCLASSIFIED  
ORNL-LR-DWG 76889

Fig. 26. Cross section and, below, side view of magnets used to impart Z-motion to the ions in passing from one layer to the next.

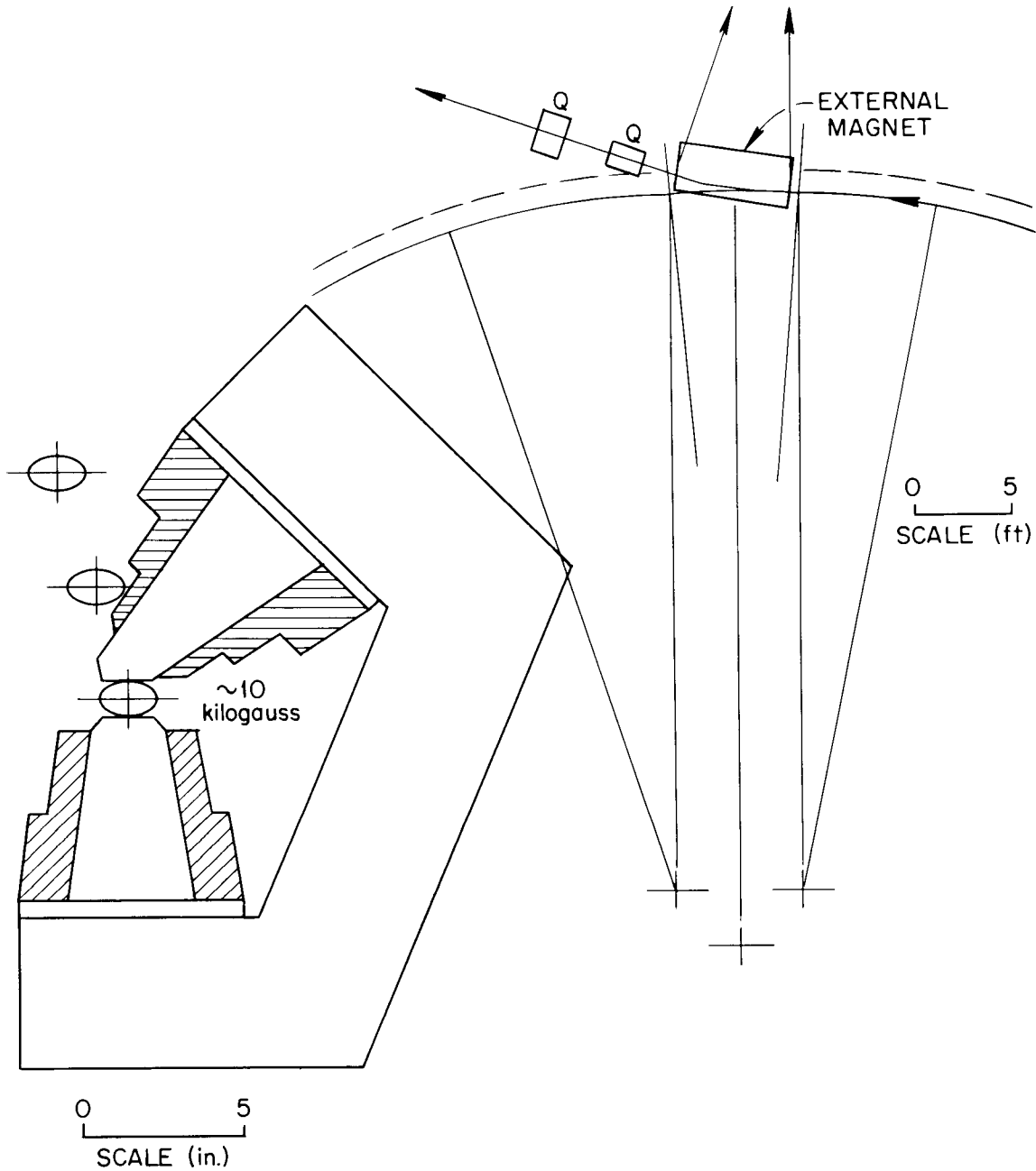
UNCLASSIFIED  
ORNL-LR-DWG 76890

Fig. 27. Plan view of machine showing location of extraction magnet in relation to orbiting beam. A cross-section of the extraction magnet is also shown.

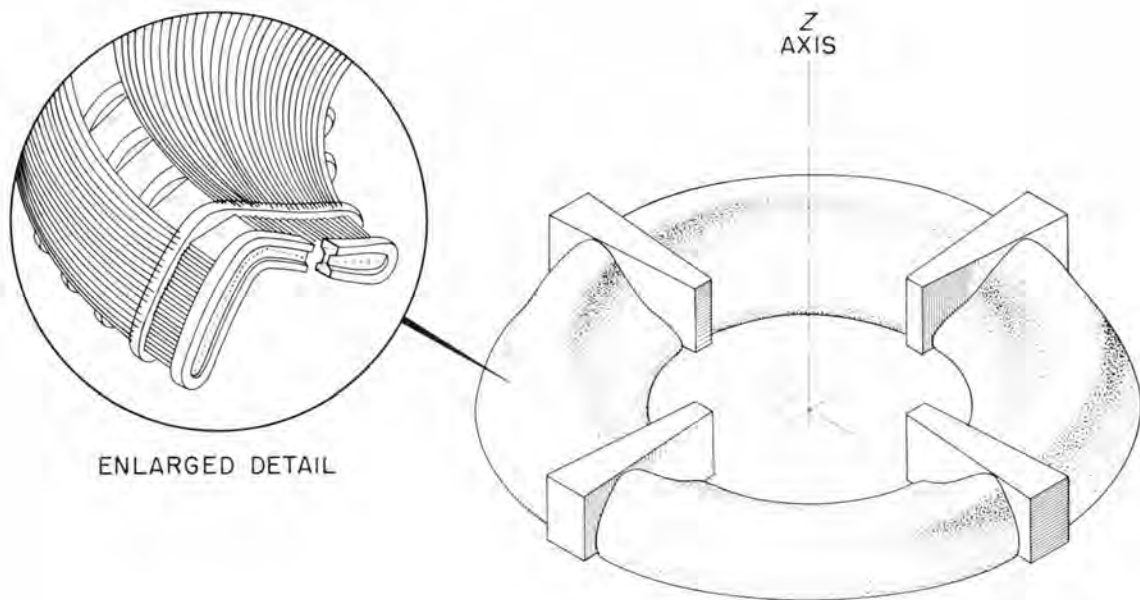
UNCLASSIFIED  
ORNL-LR-DWG 76891

Fig. 28. Artist's sketch of whole machine showing location of wedge sections and the folded nature of the machine. The insert shows details of the rf cavities, the coils, and the arrangement of the magnet stacks.

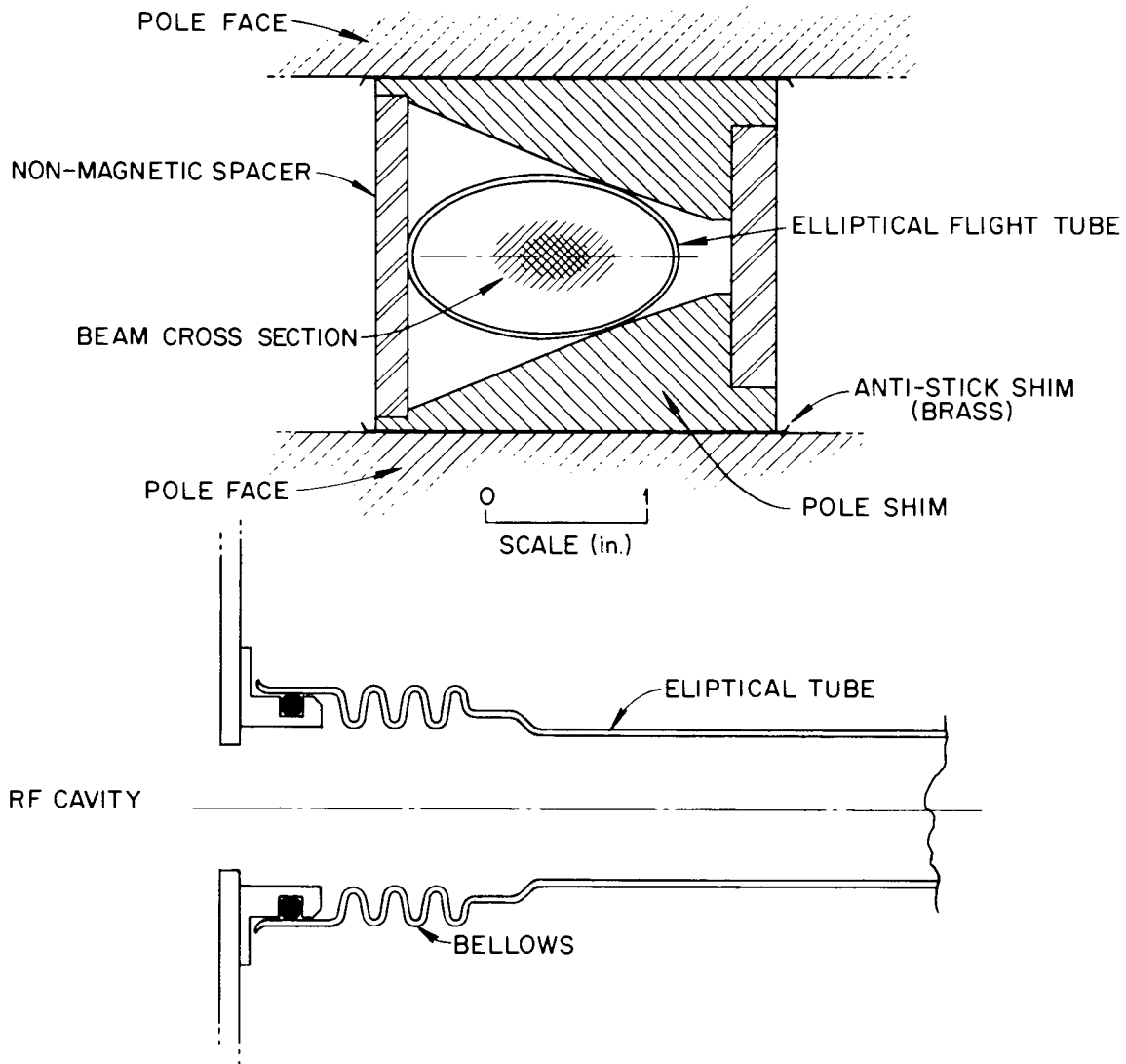
UNCLASSIFIED  
ORNL-LR-DWG 76892

Fig. 29. Above: Cross section through one magnet shim showing possible method of construction from four pieces, tack welded together. The beam pipe, held firmly in place between the parts forming the shim, could be sealed to the rf cavity vacuum envelope by the seal arrangement shown in lower figure.

UNCLASSIFIED  
ORNL-LR-DWG 76893

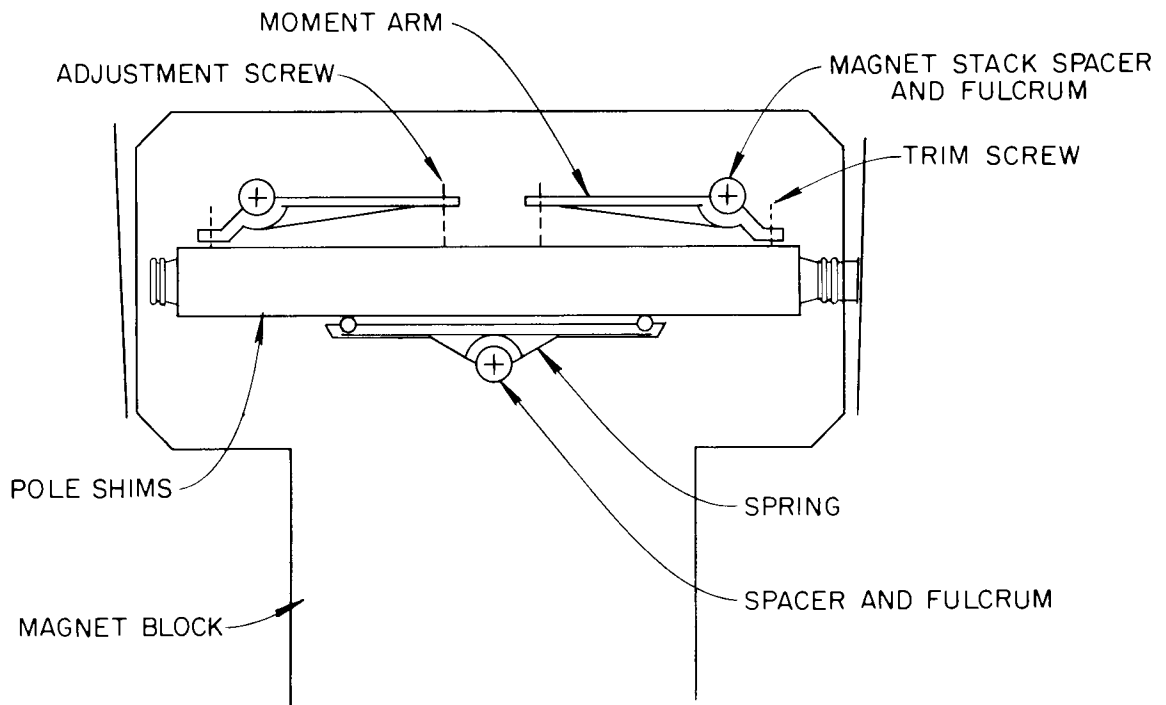


Fig. 30. Plan of one magnet stack piece showing location of magnet shim and beam pipe end seals. The shim is positioned by means of two adjustable, pivoted levers pushing against the ends of the shim unit. A pivoted spring provides the reaction. This arrangement permits both radial and differential motion of the shim in relation to the machine.

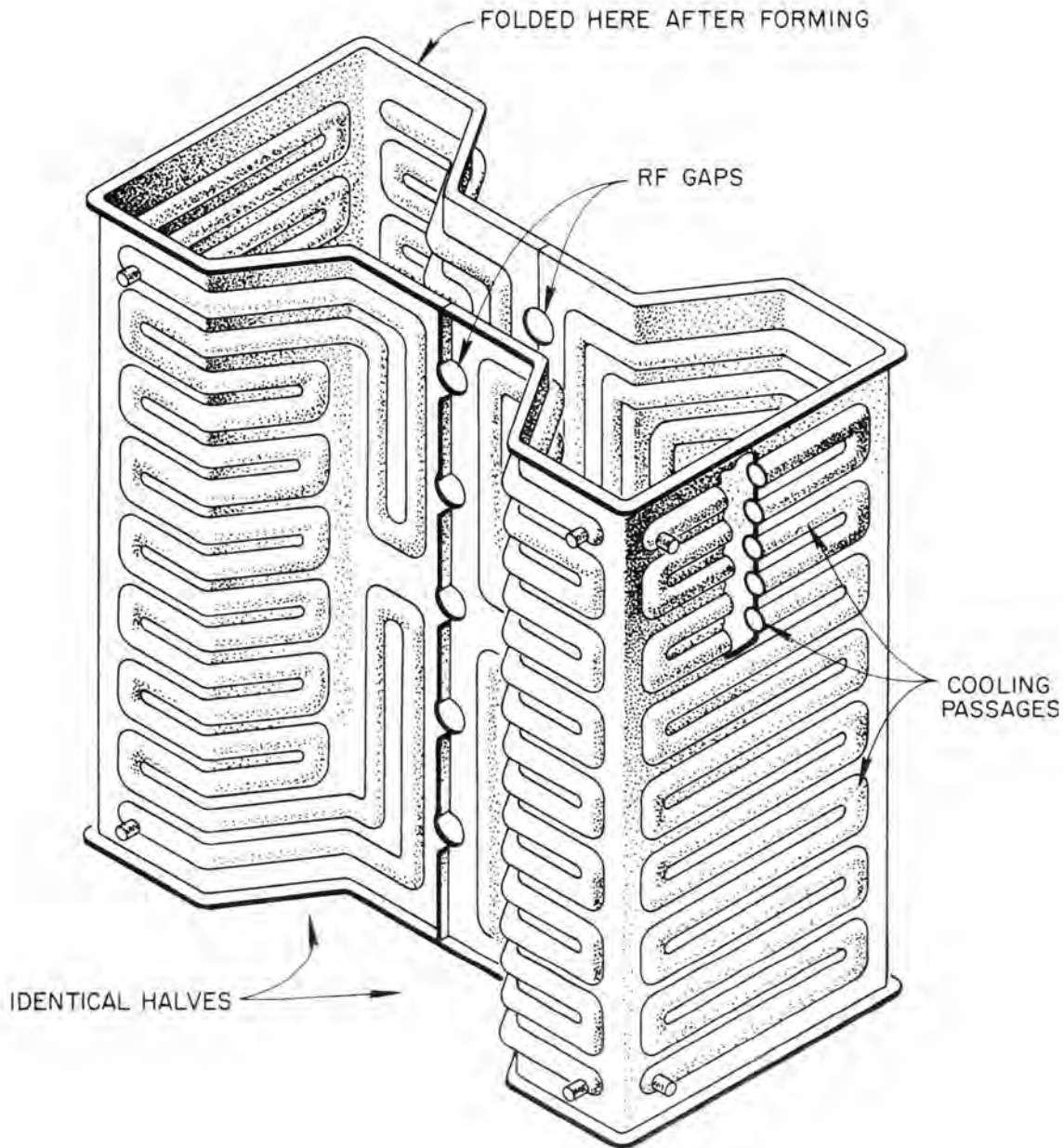


Fig. 31. Part of the liner forming the rf cavity. Multiple cooling passages are used to increase the rigidity of the structure and to reduce the surface electrical resistance. Many such pieces could be tack-welded together to form a complete cavity. A suitable material for these units is called "Hole-in-strip" copper sheet.

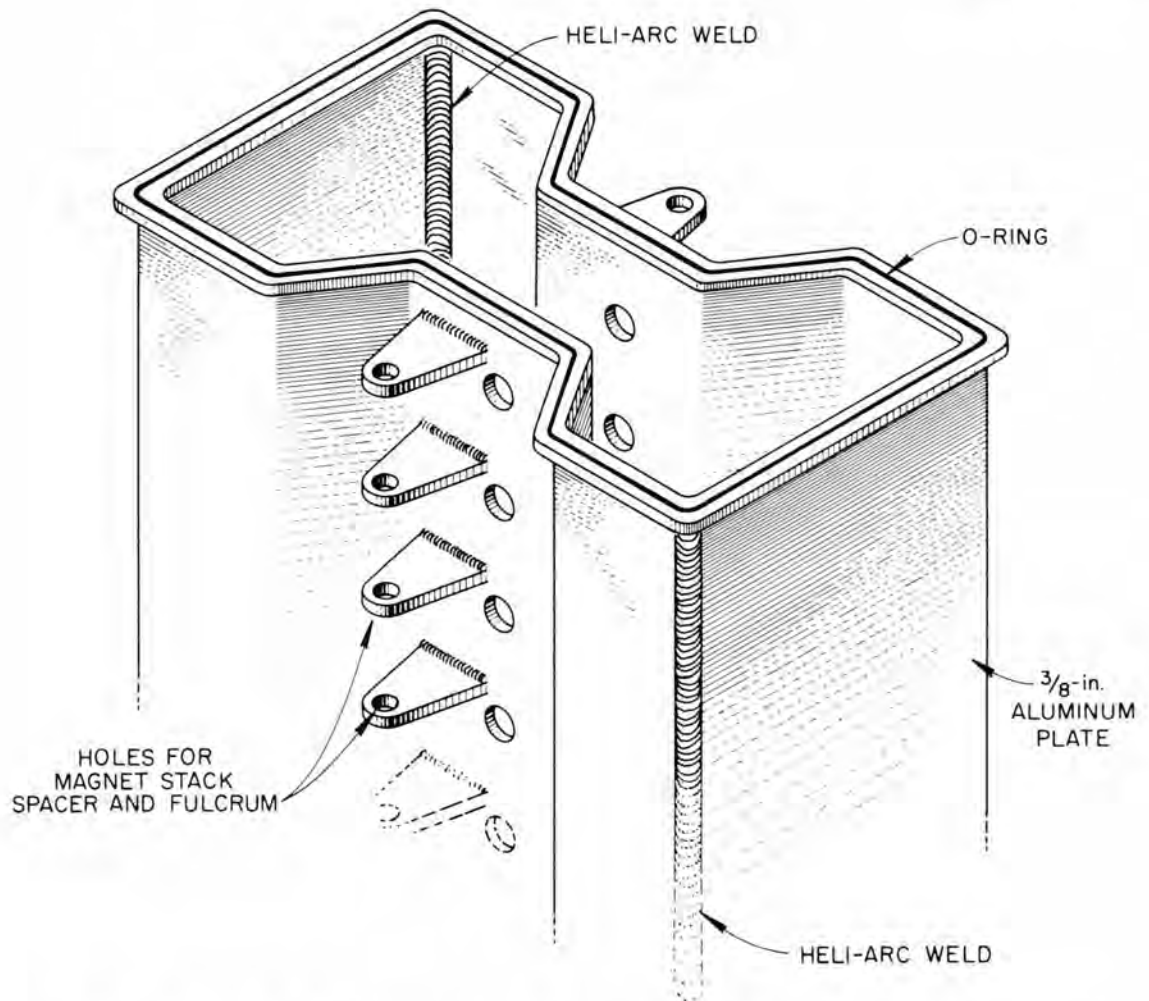
UNCLASSIFIED  
ORNL-LR-DWG 77367

Fig. 32. Part of outer vacuum vessel for the rf liner. Aluminum would be a suitable construction material.

### 13. 1. A Developed Design for a 120-MeV to 1-GeV SOC.

The design developments discussed above make it possible to calculate the design parameters for an improved second-stage SOC for the accelerator system described in Section 12. The major changes from the parameters of magnet described in Table II are, of course, in the coil structure, as shown in Fig. 23 and 25. The new magnet details are given in Table VI. Features of the radio-frequency system are shown in Fig. 23, 24, and 25, and the details are given in Table VII.

As shown in Fig. 26 four pairs of z-motion magnets are introduced, on both the rising and falling sections. The numbers given in Table VIII are for the falling (outer)side; the other set should be very similar in power, weight, and cost. The details for the extraction magnet shown in Fig. 27 are listed in Table IX.

Table VI. Magnet Parameters for a Developed 120-MeV to 1-GeV SOC.

Height (ft)			7.5
2 N (number of cells/turn)			100
Number of turns			60
$r_o$ , cyclotron unit (in.)			555
$B_o$ (kG)			2.25
	<u>at 120 MeV</u>	<u>at 400 MeV</u>	<u>at 1 GeV</u>
r (in.)	257	392	480
B (kG)	4.50	4.49	4.88
Length of ion path (ft)	-	3,725	12,955
dB/dr (kG/in.)	3.0	-	2.5
n	170	-	245
DA (in.)	1.5	1.0	1.0
Width, mean (in.)			6
DM (in.)			1.5
DC (in.)			0
Magnet steel, less shims (tons)			530
Support structure (tons)			290
<u>Magnet Coils</u>			
Number, 60 in each quadrant			240
Cross-section area, 2.5 x 3.5 (in. <sup>2</sup> )			8.7
Form factor			0.7
Resistance (ohm/ft)		$1.34 \times 10^{-6}$	
Length, plus two image coils (ft)		16,600	
Total power (MW)			2.25
Weight of copper, with image coils (ton)			263

Table VII. RF System for Developed 120-MeV to 1-GeV SOC

$f_r$ , frequency in cavities (Mc/s)	191
Number of cavities	100
Total number of accelerators, in 60 turns	6000
Energy gain, mean (keV/gap)	147
Power loss of cavity (kW/ft)	3.8
Power loss of cavity corrugated (kW/ft)	3.0
Cavity spacings	
2g (in.)	4.0
A (in.)	4.0
B (in.)	8.0
C (in.)	12.0
Length of each cavity (ft)	25
Electric field strength in cavity (kV/in.)	37
Total power loss to cavities, at $\phi_s = 0^\circ$ (MW)	9.5
Loss to cavities, corrugated walls ( $\phi_s = 0^\circ$ ) (MW)	7.6
Loss to cavities, corrugated walls ( $\phi_s = 20^\circ$ ) (MW)	8.1
Beam loading at 1 mA, mean (MW)	0.88
Beam loading at 10 mA, mean (MW)	8.8
Surface area of cavities (ft <sup>2</sup> )	15,700

Table VIII. Z-Motion Magnets, see Fig. 26

Field strength, mean (kG)	5.0
Gap, mean (in.)	1.5
Number of gaps/magnet	30
Weight, each (tons)	8
Weight, four pairs (tons)	64
<u>Coils</u>	
Cross-section area, 3 x 5 in., (in. <sup>2</sup> )	15
Form factor	7
Power loss, each (kW)	8.7
Power loss, total (kW)	70.0
Total weight, copper (tons)	11.5

Table IX. Extraction Magnet, see Fig. 27

---

Length (in. )	70
Gap, mean (in. )	1.0
Width, mean (in. )	2.0
Field strength, mean (kG)	10.0
Gradient, probably	0
Weight (tons)	2.4
<u>Coil</u>	
Cross-section area (in. <sup>2</sup> )	8
Form factor	0.7
Efficiency	0.9
Power, total (kW)	16.2
Weight, copper (tons)	-

---

### 13.2. Cost Estimate for 1-GeV SOC System, Developed Design.

The improvements in the developed design for the second-stage SOC, described above, significantly reduce the cost of the machine. The cost estimate for the developed second-stage is itemized, along with pertinent assumptions, in Table X. The total estimated cost is under  $\$9.4 \times 10^6$ ; the comparable estimate for the basic design was  $\$11.4 \times 10^6$ , see Table VI, page 43.

The author assumes sole responsibility for the cost estimates given here.

The cost estimate for the complete accelerator system, as outlined in Table I, designed to provide a 1-mA beam of 1-GeV protons is summarized below:

1. Cockcroft-Walton injector (0.5 MeV)	$\$ 0.25 \times 10^6$
2. Linac (15 MeV)	1.48
3. First-Stage SOC (15-120 MeV)	1.92
4. Second-Stage SOC (120 MeV - 1 GeV)	9.31
	<hr/>
	12.96
Contingency, 20%	2.59
	<hr/>
TOTAL, Complete Accelerator	$\$15.55 \times 10^6$

Table X. Cost Estimate for Developed Second-Stage SOC

<u>Magnet Steel (\$0.50/lb)</u>		
For stacked magnet blocks		\$ 530 x 10 <sup>3</sup>
Support and spacing structure		290
<u>Main Magnet Coils (\$3.50/lb)</u>		1,960
<u>Motor Generators, installed (\$120/kW)</u>		280
<u>Pole Shim Assemblies</u>		
Machined shims (\$1/lb)	\$100 x 10 <sup>3</sup>	
Working (\$1/lb)	100	
Spacers (\$1/lb)	40	
Jigs, for assembly	20	
Stainless flight tube (\$3/ft)	40	
Bellows ends (\$5/end)	60	
Vacuum connections (\$10/gap)	60	
Magnet spacers (\$1/each)	18	
Adjustment arms (\$3/each)	36	
Spring (\$5/each)	30	
		504
<u>Z-Motion Magnets</u>		
Steel	130	
Coils	160	
Power supply	20	
		310
<u>Extraction Magnet</u>		
Steel	3	
Coils	3	
Power supply	2	
		8
Partial total, carried over to next page		\$3,882 x 10 <sup>3</sup>

Table X, Cont'd.

Carried over from previous page		\$3,882 x 10 <sup>3</sup>
<u>RF Cavities</u>		
Outer vacuum vessel		
Aluminum plate, 3/8 in. (\$3.50/ft <sup>2</sup> )	50 x 10 <sup>3</sup>	
Flanges and seals	60	
Fabrication (welding at \$3/linear ft)	100	
Supports and ties	20	
Vacuum connections	10	
RF liner (except ends and elbows)		
Copper sheet, 3/16 in. (\$12/ft <sup>2</sup> )	190	
Development of passages and connections	100	
Fabrication (welding at \$5/linear ft)	100	
Feed lines and couplings	50	
Tuning mechanism	50	
Liner ends (\$150/ft <sup>2</sup> )	190	
Elbows (\$100/ft <sup>2</sup> )	240	
		\$1,160
<u>RF Parts</u> (\$130/kW)		1,170
<u>RF Power Supply</u> (\$100/kW, 60% eff.)		1,350
<u>Tubes</u> (\$100/kW)		900
<u>Vacuum</u> , pumps and piping		100
<u>Controls</u> , magnet, rf, phasing, correlation		500
<u>Mechanical Monkey</u> , mechanical control, etc.		200
<u>Beam Transport</u> , from 1st to 2nd SOC		50
<hr/>		
Total cost for developed 120-MeV - 1-GeV SOC		<u>\$9,312 x 10<sup>3</sup></u>

13.3. Three Types of High-Intensity Accelerators (Meson Factories) Briefly Compared.

Brief Comparison Between Three Types  
of Meson Factories

	<u>SOC (ORNL)</u>	<u>Yale Linac</u>	<u>Mc<sup>2</sup> Cyclotron (ORNL)</u>
Proposed final energy	1,000 MeV	750 MeV	810 MeV
Upper limit	> 10 GeV	>10 GeV	810 MeV
Proposed mean current	1.0 mA	1.0 mA	100 $\mu$ A
Upper limit	10 mA	1.0 mA	1.0 mA
Extraction efficiency	100%	100%	80%
Extracted beam quality	Good	Good	Probably Good
Microscopic beam structure	5%	1.4%	5%
Macroscopic beam structure	100%	20%	100%
Energy spread in beam	0.1%	0.1%	0.1%
Cost of machine per watt of beam	\$16	\$24	\$120
Machine cost for 1 GeV at 1 mA	$\$16 \times 10^6$	Extrapolated to $\$24.2 \times 10^6$	Not Possible
Machine cost for 810 MeV, current as proposed	Interpolated to $\$13.8 \times 10^6$	$\$18.5 \times 10^6$	$\$14.5 \times 10^6$
Variable energy capability	Yes	Yes	No

Acknowledgements

The encouragement given by R. S. Livingston, E. D. Hudson, R. J. Jones, and R. S. Lord is gratefully acknowledged.

References

1. See "Section VII Meson Factories," in Proceedings of the International Conference on Sector-Focused Cyclotrons, Nucl. Instr. and Meth. 18-19, 387-478 (1962).
2. Russell, F. M., "A Fixed-Frequency, Fixed-Field, High-Energy Accelerator," Nucl. Instr. and Meth. (submitted).
3. Courant, E. D. and Snyder, H. S., "Theory of the Alternating Gradient Synchrotron," Annals of Physics 3, 1 (1958).
4. Jones, R. J., "Remarks on Tune-up of Analogue II," Nucl. Instr. and Meth. 18-19, 469-471 (1962).
5. Rose, M. E., "Focusing and Maximum Energy of Ions in the Cyclotron," Phys. Rev. 13, 392 (1938).
6. The Mc<sup>2</sup> Isochronous Cyclotron. A Status Report, June 15, 1962, ORNL-3324.
7. Howard, F. T., "Catalogue of Isochronous Cyclotrons," Nucl. Instr. and Meth. 18-19, 125 (1962).

ORNL-3431  
UC-28 - Particle Accelerators and  
High-Voltage Machines  
TID-4500 (20th ed.)

## INTERNAL DISTRIBUTION

1. Biology Library
- 2-4. Central Research Library
5. Reactor Division Library
6. Laboratory Shift Supervisor
- 7-8. ORNL - Y-12 Technical Library  
Document Reference Section
9. Laboratory Records, ORNL - RC
- 10-200. Laboratory Records Department
- 201-210. Accelerator Information Center
211. C. R. Baldock
212. R. S. Bender
213. R. D. Birkhoff
214. C. J. Borkowski
215. J. C. Bresee
216. G. L. Broyles
217. H. O. Cohn
218. R. J. Cox
219. J. L. Fowler
220. C. B. Fulmer
221. W. M. Good
222. C. D. Goodman
223. E. E. Gross
224. C. S. Harrill
225. F. T. Howard
226. E. D. Hudson
227. R. J. Jones
228. C. E. Larson
229. R. S. Livingston
230. R. S. Lord
231. L. O. Love
232. F. C. Maienschein
233. J. E. Mann
234. M. B. Marshall
235. J. A. Martin
236. Axel Meyer
237. S. W. Mosko
238. E. Newman
239. E. L. Olson
240. E. G. Richardson, Jr.

- 241. A. W. Riikola
- 242-252. F. M. Russell
- 253. J. A. Russell
- 254. H. E. Seagren
- 255. L. B. Schneider
- 256. E. D. Shipley
- 257. M. J. Skinner
- 258. W. R. Smith
- 259. A. H. Snell
- 260. J. A. Swartout
- 261. J. E. Turner
- 262. A. M. Weinberg
- 263. W. H. White, Jr.
- 264. R. E. Worsham
- 265. N. F. Ziegler
- 266. A. Zucker
- 267. D. L. Judd (consultant)
- 268. B. L. Cohen (consultant)
- 269. M. Deutsch (consultant)
- 270. A. M. Clogston (consultant)
- 271. L. J. Rainwater (consultant)
- 272. J. A. Wheeler (consultant)

#### EXTERNAL DISTRIBUTION

- 273-274. Research and Development Division,  
AEC, ORO
- 275-811. Given distribution as shown in TID-4500 (20th ed. )  
under Particle Accelerators and High-Voltage  
Machines (75 copies - OTS).